International Journal of Nanomedicine

Dovepress
Taylor & Francis Group

Open Access Full Text Article

ORIGINAL RESEARCH

Targeting Acne: Development of Monensin-Loaded Nanostructured Lipid Carriers

Fatima Abid[1], Sangseo Kim[1], Bhumika Savaliya[2], Laura Cesari[3], Marzieh Amirmostofian[1], Sadikalmahdi Abdella[1], Darren J Trott[2], Stephen W Page[4], Sanjay Garg[1]

[1]Centre for Pharmaceutical Innovation, Clinical and Health Sciences, University of South Australia, Adelaide, SA, 5000, Australia; [2]Australian Centre for Antimicrobial Resistance Ecology, School of Animal and Veterinary Sciences, University of Adelaide, Roseworthy, SA, 5371, Australia; [3]Faculty of Pharmacy, Aix-Marseille Université, Marseille, 13007, France; [4]Luoda Pharma, Newtown, NSW, 2042, Australia

Correspondence: Sanjay Garg, Centre for Pharmaceutical Innovation, Clinical and Health Sciences, University of South Australia, Adelaide, SA, 5000, Australia, Email Sanjay.garg@unisa.edu.au

Purpose: The emergence of antimicrobial resistance (AMR) has made treating acne vulgaris increasingly challenging, thus underscoring the urgent need for new antibacterial therapies. This research aimed to discover, for the first time, the efficacy of monensin (MON) against acne pathogens by encapsulating MON in nanostructured lipid carriers (NLCs) to achieve targeted topical delivery.

Methods: MON-loaded NLCs were formulated and optimized using the Design of Experiments (DoE) approach and incorporated in a gel formulation. The potential of MON, MON-NLCs, and its gel formulation was investigated against resistant human isolates of *C. acnes, Staphylococcus aureus* (*S. aureus*), and *Staphylococcus epidermidis* (*S. epidermidis*) using the agar dilution method. Using the porcine ear skin, the ex vivo deposition of MON was evaluated in different skin layers. The cytotoxicity assay was also performed at antibacterial concentrations using the keratinocyte cell line.

Results: MON-loaded NLCs were developed using stearic acid, oleic acid, and Tween® 80 and optimized with particle size, polydispersity index, and zeta potential of 96.65 ± 0.94 nm, 0.13 ± 0.01, and −36.50 ± 0.30 mV, respectively. The ex vivo deposition experiments showed that MON did not penetrate any skin layer using its water dispersion. However, a significant amount of MON was deposited into the epidermal layer using MON-NLC (4219.86 ± 388.32 ng/cm²) and gel formulation (8180.73 ± 482.37 ng/cm²), whereas no MON permeated to the dermis layer using gel formulation. The antibacterial study revealed the potential of MON, MON-NLC, and gel formulation against *C. acnes* isolates (MIC range 0.125–4 µg/mL, 0.25–4 µg/mL, and 0.125–1 µg/mL respectively). The cell viability results suggested MON-NLC formulation as a safe topical treatment effective at antibacterial concentrations.

Conclusion: This research highlights the novel ability of MON against resistant acne-causing pathogens and the potential of MON-NLCs to deliver MON to the targeted epidermal skin layer effectively.

Keywords: acne vulgaris, antibiotic discovery, topical gel, nano lipid carriers, monensin

Introduction

Antimicrobial resistance (AMR) is a critical global public health concern, ranked among the top three public health issues, responsible for over 1 million deaths worldwide.[1–3] AMR is a natural phenomenon that results from the rapid genetic evolution of microorganisms to existing antimicrobial therapies, including antibiotics, making treatments ineffective and leading to prolonged illness, increased mortality, and the emergence of difficult-to-treat infectious diseases.[2,4–7] Human activities, particularly the prolonged overuse and misuse of antimicrobials, exacerbate the spread of AMR, posing a serious threat to prevent or treat infections.[7,8] The problem of AMR has been emerging since the 1970s in treating one of the most prevalent skin conditions, acne vulgaris, mainly caused by hypercolonization of *Cutibacterium acnes* (*C. acnes*), for which antibiotics serve as the cornerstone of treatment.[3,9] However, the increasing resistance of *C. acnes* strains jeopardizes the efficacy of current acne therapies, underscoring the urgent need for the development of novel antibacterial interventions.

Received: 15 October 2024
Accepted: 4 February 2025
Published: 19 February 2025

Monensin (MON) is a naturally occurring ionophore antibiotic produced by *Streptomyces cinnamonensis*,[10] known to exhibit anticoccidial and antimicrobial properties.[11–15] Its effect against the gram-positive *Staphylococcus aureus* (*S. aureus*) and *Staphylococcus epidermidis* (*S. epidermidis*), the bacterial isolates known for causing acne, has been reported previously.[16,17] However, to the best of our knowledge, its effect has never been investigated against the human *C. acnes* pathogen. Since acne bacteria reside in the hair follicle epithelium,[18] the topical route is preferred for acne treatments as it helps reduce the risk of systemic side effects.[19] However, skin provides a physical barrier for permeating active compounds with high molecular weight (>500 g/mol)[20] to target the site and achieve therapeutic effects.[21] MON is a highly lipophilic compound[22] with a molecular weight of 670.871 g/mol, and therefore, its administration on the skin can limit its dermal application.

The studies investigating the delivery of compounds to the skin primarily emphasize nanocarriers as innovative drug delivery systems that have shown considerable promise in topical administration, enhancing drug permeation through the skin barrier to reach the hair follicles in the epidermal skin layer.[19,23–25] Various nano-drug delivery systems have been reported previously for acne therapy, including lipid nanocarriers comprising nanostructured lipid carriers (NLCs),[26–28] solid lipid nanoparticles,[29–33] nanoemulsions,[34–38] liposomes,[39,40] polymeric nanomicelles,[41,42] and microemulsions.[43–46] Among recent investigations focusing on nanoparticles for targeted delivery to hair follicles, NLCs have emerged as particularly effective in improving drug permeation to hair follicles and enhancing drug loading efficiency, thereby reducing the adverse effects associated with dosage.[47–51]

NLCs are the second generation of lipid nanoparticles that serve as delivery vehicles for both hydrophilic and hydrophobic drugs, featuring a solid lipid matrix combined with liquid lipids.[52] These carriers excel at immobilizing drugs and preventing particle coalescence due to their solid matrix, and the inclusion of liquid oil droplets within the solid matrix enhances the capacity of drug loading.[53] Moreover, NLCs provide numerous advantages, such as minimal toxicity, reduced drug leakage, improved stability, biodegradability, shielding drugs from chemical degradation, and the ability to facilitate controlled drug release.[52] The nano-scale size of NLCs allows them to interact with the stratum corneum by creating a single-layered lipid film on the skin's surface. This interaction disrupts the tight packing of corneocytes, thus enhancing the permeation of drugs into deeper skin layers.[54–59] Through this, NLCs produce an occlusive effect, prevent water loss, enhance skin moisture levels, and aid in the permeation of drugs across the stratum corneum.[56] Additionally, the presence of surfactants within NLCs alters the skin's structure, thereby serving as enhancers of skin permeability.[60,61] To maximize the therapeutic effect of MON, it is crucial to target delivery to the hair follicular site. This can be accomplished through the development of an optimized MON-loaded NLC, which may increase skin permeability and aid the distribution of MON into the lipid-rich epidermal layer.

To our knowledge, this study pioneers the discovery of MON activity against resistant acne-causing pathogens (*C. acnes*). Also, as far as we are aware, this is the first study that has developed MON-loaded nanostructured lipid carriers, as this formulation has not been developed previously. The focus of the present research was to specifically (1) discover MON potential as an anti-acne therapeutic entity, (2) develop and optimize MON-Loaded NLCs formulation for topical administration using the design of experiments (DoE) approach as a mathematical statistical model (specifically, using the central composite design (CCD) technique to obtain the desired formulation), and lastly (3) to achieve safe targeted epidermal delivery of MON and investigating its ex vivo permeation and distribution across lipidic skin layers.

Materials and Methods

Materials

Monensin (MON) and narasin (NAR) were kindly given by Luoda Pharma (New South Wales, Australia). Tween® 80, formic acid, Dulbecco's phosphate buffered saline (PBS), L-glutamine, hemin, clindamycin, penicillin/streptomycin, vitamin K1, and the antibiotic clindamycin were purchased from Sigma-Aldrich (New South Wales, Australia). Gattefossé (St Priest, France) kindly supplied Gelucire® 48/16, Compritol® 888 ATO, and Precirol® ATO 5. Abitec Corporation (Ohio, USA) provided Capmul® PG-8, Capmul® PG-12, Captex® 300 Low C6, and Captex® 500. Stearyl alcohol and oleic acid (OA) were sourced from PCCA (New South Wales, Australia), while almond and sesame oil were ordered from Medisca (New South Wales, Australia), and isopropyl myristate was ordered from Acros organics (New

Jersey, USA). Merck (Melbourne, VIC, Australia) provided methanol (HPLC-grade) and dimethyl sulfoxide (DMSO). Hydroxyethyl cellulose (HEC) was procured from Medisca (New York, USA), and MTT reagent (3-(4,5-Dimethylthiazol-2-yl)-2,5-diphenyltetrazolium bromide) was purchased from Life Technologies Australia (Mulgrave, Australia). Gibco™ HEPES (N-2-hydroxyethyl) piperazine-N-2-ethane sulfonic acid, Dulbecco's modified Eagle's medium (DMEM) high glucose, Sheep blood, Gibco™ MEM non-essential amino acids (NEAA), Brucella agar base, and fetal bovine serum (FBS) were acquired from ThermoFisher Scientific (Victoria, Australia). Beeswax and stearic acid (SA) were purchased from Chem Supply located in South Australia, Australia, and witepsol® H 5 and witepsol® E76 were obtained from IOI Oleochemical (Witten, Germany).

Analysis for MON Quantification

The Liquid Chromatography Mass Spectrometry (LC-MS/MS) analysis followed a previously established and validated procedure. Briefly, samples were analyzed using a Shimadzu 8030 TripleQuad LC-MS/MS system (Shimadzu, Kyoto, Japan). In this investigation, MON served as the analyte, while NAR functioned as the internal standard. Five microliters of each sample was injected at a flow rate of 0.3 mL/min to a Phenomenex Kinetex C18 analytical column (100 Å, 50 × 3 mm, 2.6 µm). Column temperature was maintained at 40 °C, while the syringe temperature was set to 15 °C. Mobile phases consisted of (A) milliQ water with 0.1% formic acid and (B) methanol with 0.1% formic acid. The total analysis runtime was 23 minutes, with peaks for the analyte and internal standard observed at 12.85 and 14.85 minutes, respectively.

Calibration standards of MON were prepared using 14 different concentrations (10–2000 ng/mL) for LC-MS/MS analysis. Briefly, an MON stock solution (10 µg/mL) was prepared in methanol and diluted to achieve the calibration standard concentrations. A blank and a zero-point sample were prepared using methanol and methanol with NAR as the internal standard (400 µg/mL), respectively. Quality control (QC) standards were prepared as three different concentrations of 1750 µg/mL, 125 µg/mL, and 15 µg/mL, representing low, medium, and high QC, respectively. All the samples were prepared for LC-MS/MS analysis by mixing 10 µL IS with 50 µL of samples.

Multiple reaction monitoring (MRM) technique was used for evaluation, developed by optimizing precursor ion and product ion transitions. The MRM transitions for MON were 692.8 to 675.4 (CE: 54.87) and 692.8 to 461.1 (CE: 69.74). The NAR MRM transitions were 787.0 to 431.0 (CE: −60) and 787.0 to 531 (CE: −35). The dwell time for both the monensin and narasin MRM transitions was 100.

Pre-Formulation Studies

MON Solubility in Solid Lipids

The MON solubility was investigated in different solid lipids: Compritol® 888 ATO, Gelucire ® 48/16, Beeswax, Stearic acid, Stearyl alcohol, Precirol® ATO 5, Witepsol H5 (WE5), and Witepsol E76 (WE76) under lipid melt condition. One hundred milligrams of lipids is heated to melt at 80 ◦C, and then accurately weighed quantities of MON were added in 5 mg increments in molten lipid with stirring until no drug was dissolved. The solubility of MON in lipids was observed visually.

MON Solubility in Liquid Lipids

Various liquid lipids available in the laboratory were screened for MON solubility. MON was added in excess in 5 mg increments in 1 mL oil and allowed to mix continuously for 2 days using a Ratek orbital mixer (Victoria, Australia) at 25 °C until a clear lipid solution was formed. MON solubility was noted visually, as reported previously.[62,63]

Binary Mixture (BM) Ratio Determination

The ratio between lipids (solid and liquid lipids) in the binary mixture was optimized using DSC thermal analysis and a filter paper technique as previously described.[64,65] A range of BM comprising different SA and OA ratios (10:0, 9:1, 8:2, 7:3, 6:4, and 5:5) was prepared and analyzed using a DSC 250 (TA Instruments, DE, USA) for determination of their melting onset and peak temperatures and enthalpy. In brief, each sample (5 mg) was placed and sealed in an aluminum pan and analyzed from 25 °C to 70 °C. The analysis was performed at a heating rate of 10 °C/min under nitrogen flowing

at a rate of 50 mL/min. The crystallinity index of BMs was calculated from the enthalpy values using the following equation.

$$\text{Crystallinity index}(\%) = \Delta\,\text{HBM}/\Delta\,\text{HSL} \times 100$$

where ΔHBM is the enthalpy of the BM and ΔHSL of the solid lipid.

In addition, for 1 hour, the BMs were put on a filter paper, and the presence of any droplets of oil was recorded following visual examinations.

Development of MON-Entrapped Nanostructured Lipid Carriers (NLC)

The MON-loaded NLCs were developed using lipids exhibiting maximum MON solubility (SA as solid lipid and OA as liquid lipid) and Tween 80 as a surfactant. The BM of lipids (7:3 ratio of SA and OA) containing MON 1% w/w of BM was accurately weighed and melted at 80 C. Afterwards, an appropriate quantity of surfactant (Tween 80) was dissolved in Milli Q water, maintained at 80 °C. The surfactant solution is then poured into the MON-lipid mixture under constant stirring to make a hot pre-emulsion. Using the QSonica Q500 ultrasonication instrument (CT, USA), the pre-emulsion particle size was trimmed down, and the resulting micro-emulsion was quickly cooled down in an ice bath to induce the development of NLC. A series of NLCs were developed with varying surfactant to lipid ratios and sonication time and designed using Design Expert® software, version 13 (Stat-Ease Inc., Minneapolis, USA). The DoE principal was employed to screen and optimize the concentration of surfactant and BM to prepare NLC with desired PS, PDI, and ZP. The NLCs prepared were freeze-dried and stored at 4 °C for further characterization.

Development and Optimization of MON-Loaded NLC Using Central Composite Design

To screen and optimize the independent experimental factors, namely the BM (%) concentration (X_1), surfactant concentration (X_2) (%), and the sonication time (X_3) (min), DoE was utilized using the CCD at 3 levels (low, medium, and high) and their effect was statistically analyzed on the dependent variables (particle size (Y_1), polydispersity index (Y_2), and zeta potential (Y_3)) (Table 1). Based on the ANOVA, lack-of-fit, R2 including adjusted and predicted R2, the best-fit model was determined, ranging from cubic, linear, quadratic, and two-factor interaction. Subsequently, the parameters under study were optimized by setting criteria for each variable, and the formulation was optimized using the solution exhibiting the highest desirability score close to 1.0. The significance of the model was evaluated by statistical comparisons between the predicted and observed values of each dependent variable of the optimized MON-NLC formulation using a 95% confidence interval. The 3D response surface plots were also generated to evaluate and navigate the design space for the dependent variables. During the entire experiment, the solid-to-liquid lipid ratio was fixed at 7:3.

Table 1 Experimental Variables and Parameters Used for MON-NLC Preparation Using CCD by DoE

Independent variables	**Level**		
	Low	**Medium**	**High**
X_1 (% w/v)	3	4.5	6
X_2 (% w/v)	5	7.5	10
X_3 (min)	2	4	6
Fixed experimental factors			
Sonication amplitude (%)	35%		
Dependent variables	**Constraints**		
Y_1 (nm)	In range (27.83 to 100)		
Y_2	Minimum		
Y_3 (mV)	In range (−41.9 to −30)		

Notes: X_1, BM concentration; X_2, surfactant concentration; X_3, sonication time; Y_1, particle size; Y_2, polydispersity index; and Y_3, zeta potential.

Characterization of MON-Loaded Nanostructured Lipid Carriers

Particle Size, Polydispersity Index, and Zeta Potential Determination

Dynamic light scattering (DLS) analysis was performed using the Malvern Instruments Zetasizer (Worcestershire, UK) to assess the PS, PDI, and ZP of each NLC. A 200-fold dilution of samples was done with MilliQ water before taking the measurements in triplicates at 25 °C temperature.

Determination of Entrapment Efficiency (EE) and Drug Loading (DL)

EE and DL of the optimized MON-NLC formulation were determined using the previously reported method of centrifugation.[66] To obtain this, the MON-NLCs were centrifuged for 1 hour at 13000 rpm at 4 °C temperature; the supernatant was collected and filtered using a syringe filter (0.22 µm pore size), transferred to the LCMS vials, and analyzed using the LCMS method. The following equations[67] were used to evaluate the EE and DL of the optimized MON-NLCs:

$$\mathrm{EE}(\%) = \frac{\text{Total drug content} - \text{amount of free drug in the supernatant}}{\text{Total drug content}} \text{ x } 100$$

$$\mathrm{DL}(\%) = \frac{\text{Total drug content} - \text{amount of free drug in the supernatant}}{\text{Total amount of lipid}} \text{ x } 100$$

Differential Scanning Calorimetry (DSC)

To evaluate the thermal characteristics of the samples, namely MON, stearic acid (SA), oleic acid (OA), MON-SA physical mixture, and lyophilized samples of blank NLC and MON-NLC, the Discovery DSC 2920 TA Instrument (New Castle, DE, USA) was employed. Each sample, weighing approximately 4 mg, was transferred and crimp-sealed into an aluminum pan. Under a continuous nitrogen gas (flowing at a rate of 50 mL/min), the samples were subjected to heat at a rate of 10 °C/min from 25 °C to 400 °C.

Fourier Transform-Infrared Spectroscopy (FTIR)

FTIR spectra were obtained for MON, SA, MON-SA physical mixture, lyophilized MON-NLC, and lyophilized blank NLC using an ATR-FTIR spectrometer (Perkin Elmer spectrum, Massachusetts, USA). Briefly, each powdered sample was placed on the instrument in small quantities on the ATR diamond crystal and secured by applying force using clamps. The spectra were recorded between the frequency range of 400 to 4000 cm^{-1} and a resolution of 4 cm^{-1} with 16 scans per analysis. Background correction was done before each spectra recording.

Preparation of MON-NLC Gel Formulation

Among the previously evaluated gel-forming polymers for topical application,[42] HEC was used for formulating MON-NLC loaded gel. Briefly, the gel was prepared by adding 1.5% (w/v) of HEC into the optimized MON-NLC solution (0.27% w/v) and continuously stirring on a magnetic hot plate at 50 °C. The stirring was continued for 4 h until all the HEC was dissolved, and a uniform gel was formed. The gel was kept at 4 °C for further studies.

Characterization of MON-NLC Gel Formulation

By means of a PerpHecT® pH meter with ROSS® Micro electrode supplied by Thermo Scientific (Massachusetts, USA), the pH of the prepared MON-NLC gel was measured in triplicates. The rheological behavior of the formulation was also assessed using Rheosys Merlin VR from Scientex Pty Ltd (Victoria, Australia) with a 15mm diameter parallel plate. The oscillatory shear rate sweep was performed once at a fixed temperature of 25 °C, with a shear rate range of 1–100 s^{-1}. The rate sweep measurements were carried out to assess the gel's viscosity.

Preliminary Stability Studies

The optimized MON-NLCs were also investigated for 14 days for colloidal stability by determining any changes in particle size, PDI, and ZP under storage at 4 °C.

In vitro Antibacterial Study

This study involved thirty clinical isolates of *C. acnes*, previously obtained from Dr. J. Robson at Sullivan Nicolaides Pathology (Bowen Hills, Queensland), along with *S. aureus* ATCC (American Type Culture Collection) 29213 and *S. epidermidis* ATCC 14990. Brucella agar plates supplemented with laked sheep blood (5% v/v), vitamin K1, and hemin were used to culture the *C. acnes* isolates. The plates were incubated anaerobically for 48 hours at 37 °C. Clindamycin was used to test against *Bacteroides fragilis* (*B. fragilis*) ATCC 25285 employed as a quality control strain.

Minimal Inhibitory Concentration (MIC)

The agar dilution method was utilized to determine the minimum inhibitory concentration (MIC) of anaerobic bacteria (*C. acnes* and *B. fragilis* ATCC 25285) following the Clinical Laboratory Standards Institute (CLSI) M11 guidelines.[68] At the start of this study, Brucella agar medium (supplemented with 1 μg/mL vitamin K1 and 5 μg/mL hemin) was prepared and sterilized by autoclaving. Stock solutions were made at concentrations at least 10 times higher than the highest antibacterial concentration to be tested for MON, MON-NLC, and MON-NLC gel. Methanol was used to prepare MON stock solution, while MilliQ water was used to prepare MON-NLC and MON-NLC gel. The antimicrobial concentrations were serially diluted to achieve ranges of 0.08–8 μg/mL for *C. acnes* strains and 0.125–4 μg/mL for staphylococcal strains. PBS was used to prepare MON serial dilutions, whereas MilliQ water was used for MON-NLC and MON-NLC gel. Twenty-milliliter of agar dilution plates was prepared containing laked sheep blood (1mL), 10x antimicrobial agent solution (2 mL), and molten Brucella agar (17 mL) and allowed to solidify before being inoculated by *C. acnes* and *B. fragilis* isolates. The agar plates were subcultured with the isolates twice, and a direct colony suspension was prepared to achieve the 0.5 McFarland standard of a bacterial inoculum measured using a nephelometer. Inoculum-replicating apparatus was used to apply approximately 2 μL inoculum on an agar surface, resulting in approximately 10^5 CFU/mL final inoculum concentration per spot on the agar plates. Furthermore, a control plate devoid of any bacterial inoculation to check for negative growth and another plate containing inocula but lacking antibacterial agents to serve as a positive growth control were also set up. The plates containing anaerobes were then placed in anaerobic conditions at 37°C for 48 hours using anaerobic jars containing an indicator to confirm anaerobiosis, while those with staphylococcal isolates were incubated aerobically at the same temperature for 24 hours.

MIC Determination

Following the incubation period, a visual inspection of the agar plates was done to identify any signs of bacterial growth. The value of the minimum inhibitory concentration (MIC) for each isolate was recorded as the lowest concentration at which the growth was halted. Based on MIC results achieved for *B. fragilis* ATCC 25285 (control strain) against the reference clindamycin, the performance of the test system was evaluated. No growth in negative control plates and an acceptable level of growth in positive control plates were considered to validate the tests.

In vitro Cytotoxicity Assay

The MTT assay[42] was performed to test the effect of optimized MON-NLC formulation on the viability of keratinocyte cells (HaCaT). High glucose DMEM added with 10% FBS, 1.5% HEPES, and 1% of each NEAA and Pen-Strep solution was used to subculture the cells in a T25 sterile culture flask and incubated in a humidified incubator at 37 °C under 5% CO_2. To obtain a confluency of 90%, the media was replaced every 48 hours with fresh media. The cells were subsequently placed onto 96-well plates containing 100 μL of culture media and left to incubate for 24 hours. On the following day, the test samples were introduced (100 μL) and underwent another 24-hour incubation period. A series of concentrations was tested in triplicate with a range of 0.5 to 16 μg/mL. The controls were also set up where no treatment was added to the cells. The next day, the cells were delicately rinsed twice using sterile PBS, followed by the addition of 10 μL of the MTT solution and incubated for another 4 h. Afterwards, the MTT solution was aspirated from each well, followed by the addition of DMSO to dissolve the MTT formazan crystals, and the absorbance was recorded using the Perkin Elmer Wallac microplate reader (Waltham, MA, USA) at 570 nm. The results were evaluated as percentage cell viability.

Ex vivo Permeation and Deposition Evaluation of MON-NLC-Gel

Skin Preparation

For this study, the full-thickness porcine ear skin samples were used after obtaining approval from the Animal Ethics Committee (University of South Australia, Australia) to collect and use scavenged tissues. The skin was thereafter obtained from a local slaughterhouse (South Australia, Australia) and prepared for ex vivo skin permeation and deposition assay using the following procedure. Using MQ water, the samples were rinsed, and the hair was carefully cut with the aid of a hair clipper. The ear cartilage was carefully removed from the skin, and the skin was stored at −20 C for further use.

Evaluation of Skin Integrity

Before each experiment, the skin samples were removed from −20 °C and allowed to thaw to room temperature. The skin was then cut into circular disks of 4.91 cm^2 with a thickness of 0.1 cm and tested for its integrity by measuring transepithelial electrical resistance (TEER) using an MM400 digital multimeter from Klein Tools, Australia. Afterward, the skin was put on Franz diffusion cells facing the dermis side downwards. Five-milliliter PBS was added in the receiver compartment, adjusted at pH 7.4, and allowed to reach equilibrium before measuring TEER to determine the integrity of the skin barrier. The samples displaying TEER of more than 10 kΩ were employed for the ex vivo permeation and deposition assay.[69]

Ex vivo Permeation and Deposition

The donor chamber of the Franz cell was then applied with precisely 1g of finite dose of NLC formulation (MON-NLC solution and MON-NLC gel) corresponding to 0.6 mg/cm^2 MON, and MON-water (control) corresponding to 0.006 mg/cm^2 MON. Throughout this study, the receptor chamber was maintained at 34 °C and allowed to continuously agitate using magnetic stirrers. To evaluate the amount of MON penetrated across the skin, 200 µL aliquots were collected in triplicates for each sample at predefined regular time intervals (1, 2, 4, 8, 12, and 24 hours) and analyzed using the developed LCMS method.

After the permeation studies were completed, the surface of each skin sample was carefully wiped using a cotton tip to remove excess formulation, rinsed using 10 mL MQ water, left to air-dry at room temperature for 3 h, and placed on a flat surface using a tape with the stratum corneum side exposed upwards. The stratum corneum was removed from the skin using a previously reported tape-stripping method.[42,70] For this purpose, fifteen D100 D-Squame sampling discs were used. Each disc was placed over the skin surface, and a firm pressure was applied for 5 seconds using a D500 pressure instrument (D-Squame®) before removing the discs using forceps. Subsequently, the forceps were used to carefully remove the epidermis layer, and the leftover skin was cut into smaller pieces to quantify MON deposition in the dermal layer. No additional techniques, such as heat, were required to separate the epidermis layer from the rest of the skin. Methanol (10 mL) was used as an extraction media[42] to obtain the amount of MON deposited in each skin layer. The extraction was performed for 24 hours by soaking the skin samples in extraction media under continuous stirring. The sample extracts were then centrifuged using Beckman Coulter centrifuge equipment (Allegra X-12R, USA) for 20 min at 3500 rpm, filtered using a syringe filter (0.45 µm pore size), and analyzed using the LC-MS/MS method.

Statistical Analysis

In this study, the average values, along with their standard deviations (SD), were derived from three separate experiments unless stated otherwise. ANOVA was used to establish statistical distinctions between the samples (control and treated), and using version 9.4.1 of the GraphPad Prism software (CA, USA), the statistical analysis was conducted to assess significance at $p < 0.05$.

Results and Discussion

Excipient Selection

Screening of Solid and Liquid Lipid

The lipids were selected based on the solubility and homogeneity of MON dissolved in different liquid lipids and solid lipids, respectively. MON solubility in various lipids was carefully determined, and lipids displaying maximum solubility were selected for NLC formulation as solubility plays a significant role in drug EE and DL capacity in NLCs.[71] MON displayed solubility in all the solid lipids used for screening, of which bee wax, Gelucire ® 48/16, WE76, and WH5 displayed similar solubility of 12 mg/g; however, SA showed the highest solubility for MON (155 mg/g) and therefore was selected as a solid lipid for NLC preparation (Figure 1A).

Among the liquid lipids screened for MON solubility, OA showed a maximum saturation solubility of 10.5 ± 0.12 mg/mL, as shown in Figure 1B, and was therefore selected for preparing NLC. The incorporation of OA in NLC preparation for topical delivery of drugs with SA has been previously investigated.[71–75] SA is a highly lipophilic, polymorphic, 18-carbon saturated fatty acid and a primary lipid component found in animal and plant fat,[76–79] whereas OA is a mono-unsaturated 18-carbon long omega-9 fatty acid, also found naturally in animal and plant fats.[53] This lipid matrix composition affects the physicochemical properties of formulated lipid nanoparticles depending on the lipid-chain length and concentration of individual lipids, thereby influencing the enthalpy and structural transition from solid to liquid state to produce more stable and less ordered lipid crystals.[76,79–82]

Optimization of Binary Mixture of Solid Lipid and Liquid Lipid

In this study, the solid lipid and liquid lipid composition in the BM were optimized based on thermal analysis using DSC and a filter paper method.[83] The thermal analysis results (Table 2) showed that, as the OA content in the BM increased to 50%, the melt onset and melt peak temperature significantly decreased to 34.21 °C and 46.88 °C, respectively. Similarly, the crystallinity index of the BM also decreased to 49.15% at the OA ratio of 50% in the BM, although the BMs with more than 30% of OA content only showed a minor decrease in crystallinity index as it would have been close to reaching the maximum dissolution of OA in SA.[64] In addition, the endothermic peaks are also broadened and reduced in height due to OA dispersion in SA, indicating the development of imperfect lattices in BM and distortion of crystallinity (Figure 2). Such behaviors allow the NLC matrix to incorporate a greater quantity of API than solid lipid nanoparticles.[84] Determining the optimal BM composition is necessary as it can also impact the occlusive effect, entrapment efficiency,

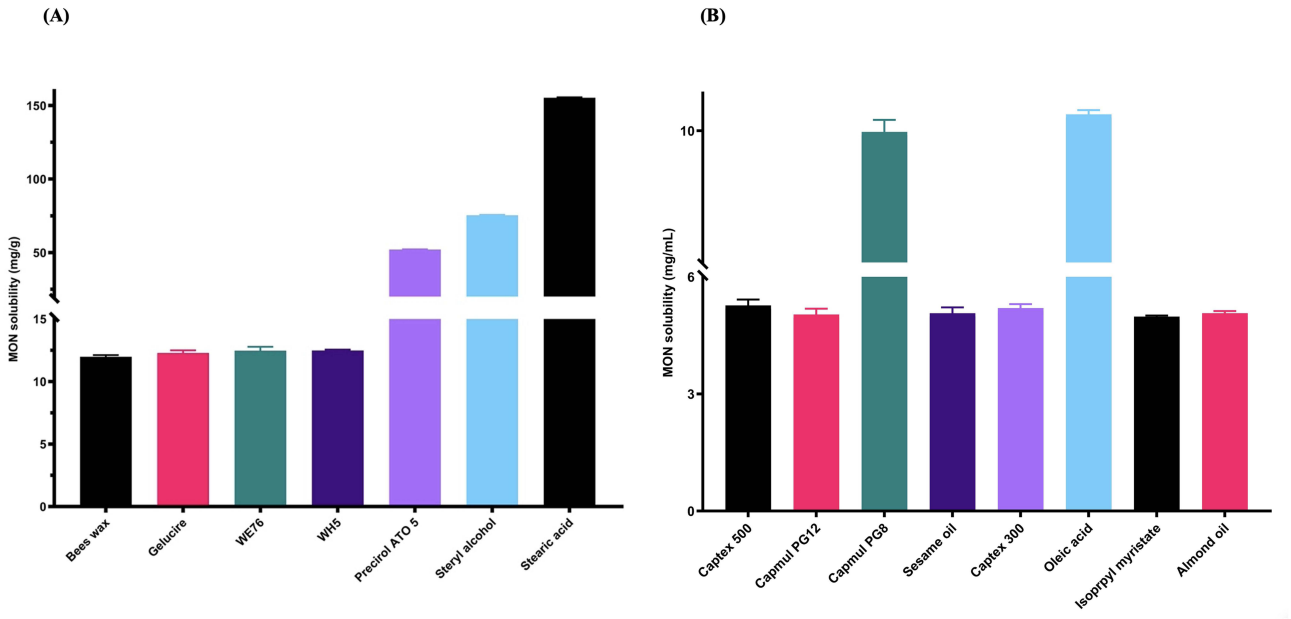

Figure 1 Solubility of MON in various (**A**) solid lipids and (**B**) liquid lipids.

Table 2 Effect of Different Ratios of Oleic Acid on BM

Binary Mixture Ratio (SA: OA)	Melt Onset Temperature (°C)	Melt Peak Temperature (°C)	Enthalpy (J/g)	Crystallinity Index (%)
10:0	54.68	57.11	216.81	N/A
9:1	51.52	55.75	185.93	85.76
8:2	46.31	53.43	148.80	68.63
7:3	44.40	51.97	137.94	63.62
6:4	38.52	48.61	112.60	51.93
5:5	34.21	46.88	106.56	49.15

Abbreviations: SA, stearic acid; OA, oleic acid.

drug loading, and stability of NLCs. While adding insufficient amounts of liquid lipids in BM can lead to the formulation comprising non-uniform NLCs, high contents of liquid lipids can result in phase separation during or after the preparation of formulation.[64] In this study, the results from the thermal analysis were also complemented by a visual assessment using the filter paper technique whereby the OA content of 40% and above started showing a smear of oil droplets on the filter paper, indicating that the maximum OA content in the BM would be ideally around 30% (Figure 3). Therefore, the BM consisting of SA (70%) and OA (30%) was used for the optimization of NLC formulations.

Formulation Development and Optimization

Formulation Optimization Using a Central Composite Design

The effect of independent factors (BM, surfactant concentration, and sonication time) on the dependent variables, namely PS (Y_1), PDI (Y_2), and zeta potential (Y_3), was studied and evaluated statistically using ANOVA and optimized using the central composite design by the DoE software. The software generated 20 runs that were prepared, and the response was

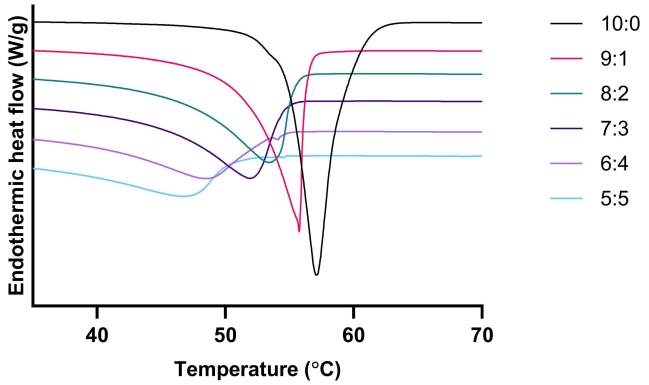

Figure 2 DSC thermogram of stearic acid and binary mixtures containing different ratios of stearic acid and oleic acid.

Figure 3 Filter papers showing a smear of oil droplets from the binary mixtures with oleic acid content above 30%.

https://doi.org/10.2147/IJN.S497108

recorded for each dependent variable (Table 3). The results demonstrated that model terms for PS, PDI, and zeta potential were all statistically significant with $p < 0.0001$. A linear model was generated for PS, whereas the variations in PDI and zeta potential were demonstrated by the quadratic models. Statistical parameters such as R^2 (including adjusted predicted R^2) and lack of fit were recorded for each model (Table 4). An acceptable correlation was found between predicted and experimental model values, as indicated by the R^2 values for each variable. The suitability of the model was further assessed by confirming the insignificance of lack of fit of each model, displaying p values greater than 0.05.[85]

Effect on Particle Size

The particle size of lipid nanoparticles is a crucial parameter as it influences the deposition and permeation characteristics of the drug across different skin layers.[30,86] Particle size below 600 nm is desirable for follicular targeting.[42,87–90] The DLS analysis showed that the PS of the MON lipid nanoparticles ranged from 27.83 nm to 134.80 nm, as shown in Table 3. A linear model was generated following regression analysis to determine the impact of independent variables (X_1, X_2, and X_3) on the particle size of MON-loaded NLCs. The particle size of MON-NLCs was significantly impacted by the BM concentration and total surfactant concentration (p-value of less than 0.05), whereas the sonication time did not have a significant effect on PS (Table 4). The effect of each independent variable on PS is also expressed by their respective coefficient values and associated

Table 3 Runs Generated by Central Composite Design and Their Measured Responses

Run	Factor 1	Factor 2	Factor 3	Response 1	Response 2	Response 3
Formulation	Binary Lipid Concentration (%)	Surfactant Concentration (%)	Sonication Time (min)	Size (nm)	PDI	Zeta Potential (mV)
1	1	3	2	67.25	0.230	−36.4
2	2	5	4.5	75.28	0.197	−32.2
3	2	5	4.5	74.02	0.211	−31.5
4	3	3	7	134.80	0.242	−41.8
5	3	3	2	101.90	0.266	−41.9
6	0.318	5	4.5	27.83	0.257	−13.5
7	2	5	4.5	74.36	0.202	−35.3
8	2	5	8.70	75.72	0.175	−31.8
9	2	1.63	4.5	121	0.371	−41.2
10	2	8.36	4.5	46.78	0.396	−11.7
11	3	7	7	99.23	0.098	−32.6
12	1	3	7	46.04	0.296	−28.1
13	2	5	4.5	80.82	0.192	−32.3
14	1	7	2	56.69	0.412	−14.2
15	1	7	7	45.1	0.211	−11.2
16	2	5	0.29	77.12	0.308	−31.9
17	3	7	2	104.80	0.447	−31
18	2	5	4.5	52.12	0.247	−33.4
19	2	5	4.5	68.04	0.214	−32.8
20	3.68	5	4.5	127	0.202	−40.6

Table 4 ANOVA Results Summary for the Dependent Variable Responses. X_1: Binary Mixture Concentration (% w/V); X_2: Total Surfactant Concentration (% w/v) and X_3: Sonication Time (Min)

	Particle Size (nm)		Polydispersity Index		Zeta Potential (mV)	
	Coefficient	***p* value**	**Coefficient**	***p* value**	**Coefficient**	***p* value**
Model		**< 0.0001**		**<0.0001**		<0.0001
Intercept	77.79		0.2110		−32.87	
X_1	28.74	**<0.0001**	−0.0138	**0.0501**	−7.54	**<0.0001**
X_2	−12.37	**0.0034**	−0.0129	0.0643	7.97	**< 0.0001**
X_3	−0.57	0.8755	−0.0536	**<0.0001**	0.7299	0.1559
X_1X_2			0.0005	0.3763	−2.38	**0.0034**
X_1X_3			0.0071	**0.0043**	−1.60	**0.0277**
X_2X_3			0.0438	**<0.0001**	−0.8750	0.1894
X_1^2			0.0002	0.5489	1.76	**0.0034**
X_2^2			0.0488	**<0.0001**	1.98	**0.0016**
X_3^2			0.009	0.2152	0.0667	0.8883
Residual						
Lack of Fit		0.2106		0.2865		0.1688
Fit statistics						
R^2	0.8254		0.9649		0.9833	
R^2 (adjusted)	0.7927		0.9333		0.9682	
R^2 (predicted)	0.7128		0.8092		0.9011	
Adequate precision	16.2567		19.4229		26.1302	

Notes: The bold values represent statistically significant values at p <0.05.

signs displayed in Table 4. The negative coefficient values suggest a negative relationship of independent variables (X_2 and X_3) on PS. A positive effect was recorded for X_1 on PS of MON-NLCs, suggesting that increasing BM concentration increases PS of the MON-NLCs, whereas increasing surfactant concentration and sonication time both reduce PS. This relationship is also showcased in the 3D response surface plot (Figure 4A). The increased PS due to increased BM concentration could be due to an increased possibility of lipid particle aggregation and an insufficient quantity of surfactant to cover the surface of lipid particles.[53,91] It was noted that by increasing BM concentration, the viscosity of the formulations also increased, which could potentially hinder the sonication process to effectively reduce the particle size, as reported previously.[92] However, increasing surfactant concentration displayed the opposite effect on the PS. The surfactant develops a dense layer around the lipid particles that reduces the surface tension between the lipid phase and aqueous phase, preventing agglomeration of particles and thereby promoting the formation of smaller particles.[53,92–95]

Effect on Polydispersity Index

The DLS measurements showed that the PDI values of the developed 20 MON-NLCs ranged from 0.098 (run 11) to 0.447 (run 17) (Table 3). The PDI provides important information about the homogeneity and uniformity of the nanoparticles in a solution, with a value lower than 0.3 indicating a uniformly distributed system. The regression analysis results showed that the model was statistically significant, with p <0.05. The PDI of the MON-NLCs was significantly impacted by the sonication time (X_3) (Figure 4B), the interaction of BM concentration and surfactant concentration with the sonication time (X_1X_3 and X_2X_3, respectively) (Table 4), and the square effect of surfactant concentration (X_2^2), as displayed in Table 4.

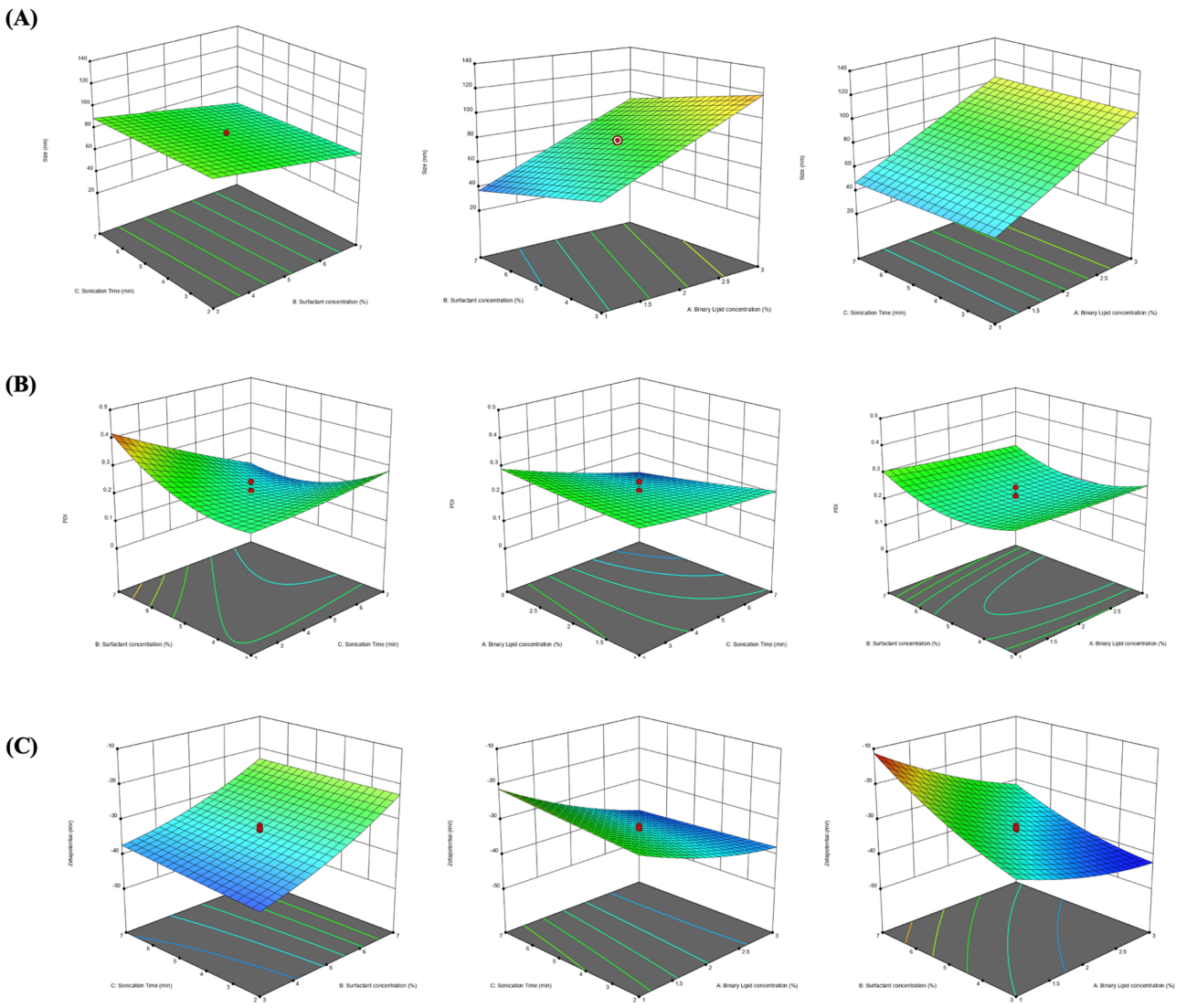

Figure 4 3D response surface plots illustrate how varying binary mixture concentration, surfactant concentration, and sonication duration affect (**A**) particle size, (**B**) polydispersity index, and (**C**) zeta potential.

The ANOVA results further revealed a significant inverse relationship between PDI, surfactant concentration, and sonication time, coinciding with previously reported studies[53,83,95] A negative relationship between PDI and BM concentration was also indicated by ANOVA; however, the effect was statistically insignificant (p=0.0501).

Effect on Zeta Potential

The stability of the nanoparticles in dispersions is attributed to their surface charge, which is an important nanoparticle characteristic used for analyzing their electrostatic properties.[96] This electrical potential, also known as ZP, is measured in millivolts and exists on the slipping plane of the electrical layers of the particles.[97] The ZP values ranging outside the range of −30 mV to 30 mV indicate the presence of strong repulsive forces between the nanoparticles, hence creating a stable colloidal dispersion.[53,98] The 20 developed lipid nanoparticle formulations showed negative ZP values, ranging from −41.9 to −11.2 mV, attributed to the presence and adsorption of highly negative charges of the SA and OA on their surfaces, resulting in overall negative charges.[53,99] The ANOVA results of the responses displayed that BM concentration and surfactant concentration had statistically significant effects on the ZP values, each having a p-value of <0.0001. Additionally, the BM concentration had a negative effect on the ZP values, and a positive effect was found with surfactant concentration on the ZP values (Figure 4C). Sonication time did not have a significant effect on the ZP values.

Table 5 Comparison of Predicted and Observed Response Values for Optimized MON-Loaded NLCs

Optimized Independent Factors	Dependent Responses	Importance	Low Predicted Value (at 95%)	Predicted Mean	High Predicted Value (at 95%)	Experimental Value
X_1, 3%	Y_1, PS (nm)	+++++ In range (27.83 to 100)	85.3511	98.633	111.915	96.65 ± 0.939
X_2, 6.18%	Y_2, PDI	+++++ Minimum (0.098 to 0.447)	0.0709	0.105334	0.1398	0.129 ± 0.011
X_3, 7 min	Y_3, ZP (mV)	+++ In range (−41.9 to −30)	−38.6055	−35.9644	−33.3233	−36.50 ± 0.300

Abbreviations: X_1, Binary mixture concentration (% w/v); X_2, surfactant concentration (% w/v); X_3, Sonication time (min); Y_1, Particle size (nm); Y_2, Polydispersity index; Y_3, Zeta potential (mV).

Optimization of MON-NLC Formulation

Criteria were set to optimize the MON-NLCs having PS ranging between 27.83 and 100 nm, minimum PDI, and ZP between −41.9 and −30 mV. The software generated a response suggesting developing a formulation with a desirability of 0.989, comprising 3% X_1 (BM concentration), 6.18% X_2 (surfactant concentration), and 7 min X_3 (sonication time) with predicted PS, PDI, and ZP of 98.633 nm, 0.105, and −35.96 mV, respectively (Table 5). A translucent solution of optimized MON-NLC was obtained (Figure 5) with a 96.65 ± 0.939 nm PS, 0.129 ± 0.011 PDI, and −36.50 ± 0.300 mV ZP (Figure 6A and B). The experimental values of PS, PDI, and ZP agreed with the predictable (Table 5), suggesting the validity of the model. Furthermore, the EE and DL of the optimized MON-NLC formulation were found to be 84.52 ± 0.48% and 1.69± 0.01%, respectively.

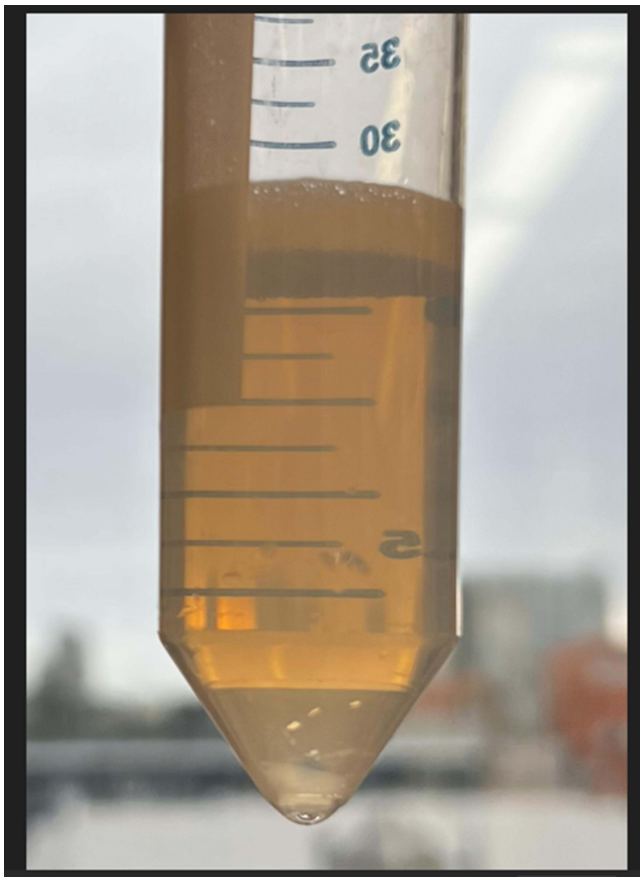

Figure 5 Optimized MON-loaded NLC.

https://doi.org/10.2147/IJN.S497108

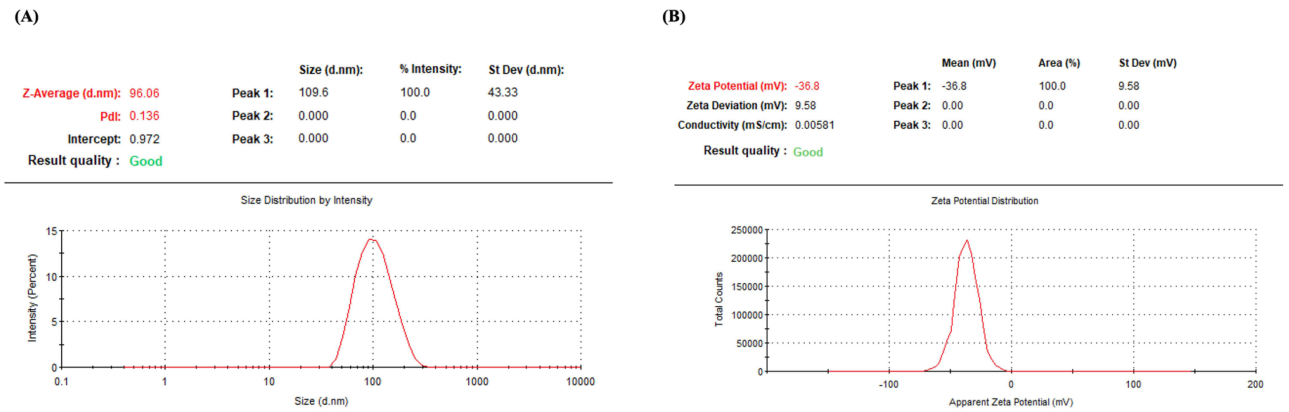

Figure 6 Optimized MON-NLC (**A**) particle size, polydispersity index, and (**B**) zeta potential.

Characterization of MON-NLCs

Fourier Transform Infrared Spectroscopy

To confirm the successful incorporation of MON into the nanostructured lipid carriers (NLCs) and investigate their molecular interactions, Fourier transform infrared (FTIR) spectroscopy analysis was performed (Figure 7). The analysis revealed the spectra of MON-NLC, BLANK-NLC, MON, SA (Stearic Acid), and PM (Physical Mixture). The FTIR spectra showed that MON displayed a characteristic peak in the region 3200–2100 cm^{-1} (Figure 7, peak 1), which corresponded to the proton vibrations in a medium-short hydrogen bond formed between the O(1) oxygen atom of the carboxylate group and O(11)H group. Additionally, a sharp peak at 1556 cm^{-1} (Figure 7, peak 2), was observed, corresponding to aromatic C=C bending.[100] Stearic acid adsorption peaks were observed at about 2915 and 2848 cm^{-1} (Figure 7, peak 3), which are attributed to −CH 2− band asymmetric and symmetric stretching vibrations, respectively. Zhu et al have reported similar findings for pure stearic acid.[101] The spectra of the physical mixture showed peaks (2915

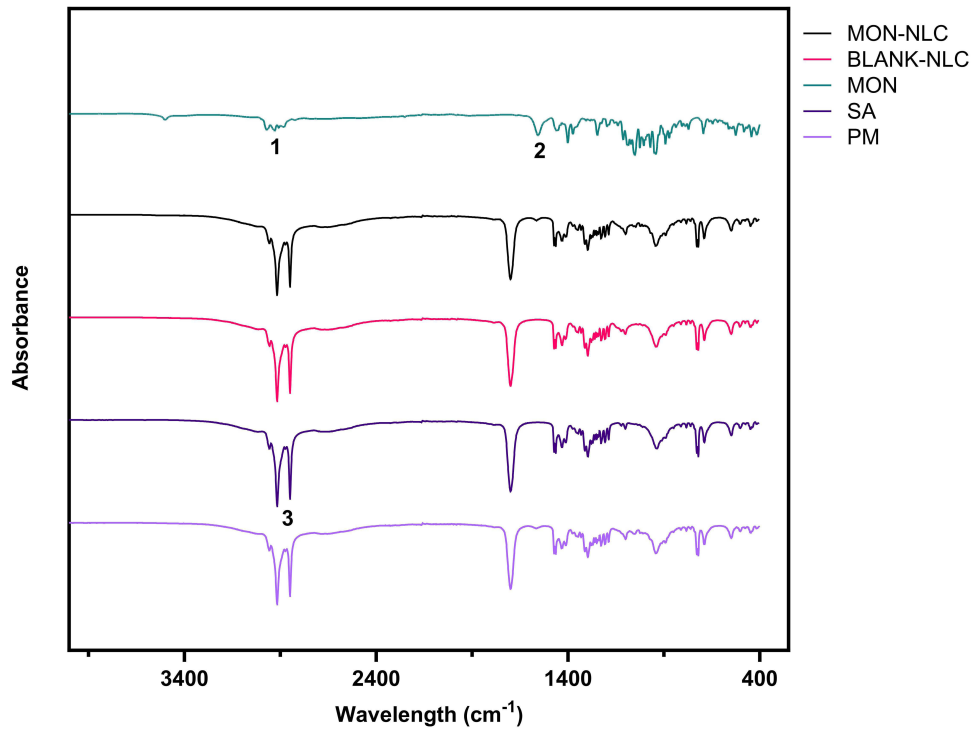

Figure 7 FTIR spectra of MON, MON-NLC, blank-NLC, SA, and physical mixture.

and 2848 cm^{-1}) corresponding to the drug and stearic acid (1556 cm^{-1}). Some peaks of MON have been masked by peaks of stearic acid, and no new peaks were observed, illustrating the absence of interaction between stearic acid and MON. The FTIR spectrum of BLANK-NLC (nanostructured lipid carriers without the MON) exhibited characteristic peaks primarily corresponding to stearic acid. The absence of peaks corresponding to the MON confirms that the Blank-NLC does not contain MON. Of note, the FTIR spectra of MON-NLC are similar to the spectra of Blank-NLC, highlighting that MON has been successfully encapsulated in the NLCs.[42,102]

Differential Scanning Calorimetry

DSC technique was used to determine the thermodynamic properties and changes in the physical state during the thermal analysis of drug-free-NLC (blank_NLC), monensin (MON), MON_NLC, pure SA, OA, and a physical mixture of SA and OA. The blank_NLC exhibited a consistent, level curve without notable thermal events, indicating an absence of phase transitions or crystallization in the blank nanostructured lipid carrier (NLC) system (Figure 8). In comparison, the MON thermogram, representing pure MON, displays distinctive thermal peaks, with the initial endothermic peak near 100 °C likely indicating water or solvent loss, while the significant peak around 300 °C signifies monensin's melting point, demonstrating its crystalline nature and thermal breakdown.[100] The MON_NLC thermogram remains predominantly flat without clear peaks, suggesting that the MON is effectively encapsulated within the NLC, modifying its thermal profile, and minimizing the expression of typical phase transitions. This implies enhanced drug stability when encased in the NLC. The thermogram of the physical mixture shows a minor endothermic peak between 50 °C and 100 °C, corresponding to the SA melting point. Beyond this point, the curve is relatively flat, suggesting a stable mixture without significant thermal transitions.

MON-NLC Gel Characterization

MON-loaded NLC gel was formulated using 1.5% HEC in 0.27% (w/v) MON-NLC solution. Blank HEC gels were screened in a previously published study[42] demonstrating that 1.5–2% HEC produces gels with adequate viscosity. Therefore, this study used 1.5% HEC concentration and assessed for rheological properties. The results demonstrated favorable shear thinning behavior of the formulated gel as shown in Figure 9. As the shear rate increased from 131(1/s) to 1178 (1/s), the viscosity of MON-NLC gel and blank gel decreased from 3.03 to 0.71 Pa.s and 3.94 to 0.92 Pa.s, respectively. The MON content in the gel formulation was 0.27% w/v (corresponding to 2.72 mg/mL MON concentration). Additionally, viscosity results showed that HEC gel possessed a high viscosity compared to the MON-NLC gel. The pH of the gel was found to be 5.85 ± 0.075, falling within the accepted pH range of 4–6 for topical products,[103] hence making it suitable for application to the skin.

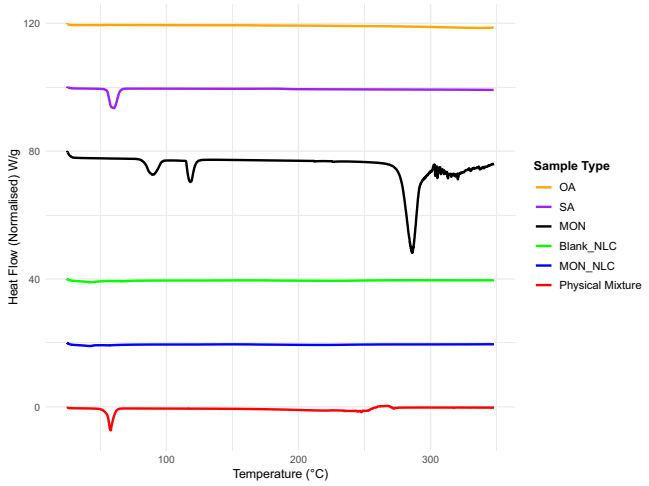

Figure 8 DSC thermograms of blank_NLC, MON (Monensin), MON_NLC, pure SA, OA, and physical mixture.

https://doi.org/10.2147/IJN.S497108

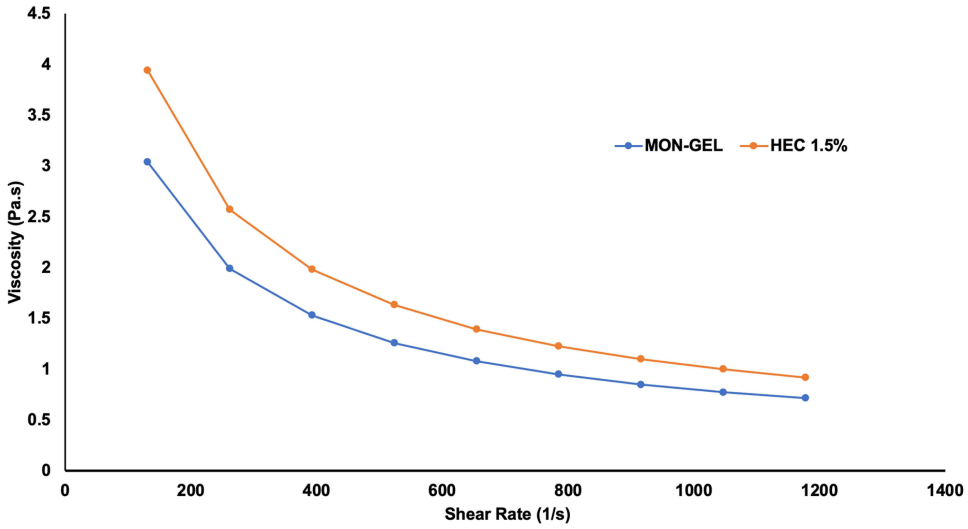

Figure 9 Rheological analysis of MON-NLC gel and hydroxyethyl cellulose (HEC) 1.5% gel.

Preliminary Stability Studies

The optimized MON-loaded NLCs were investigated for colloidal stability for two weeks under refrigerated conditions at 4 °C. Measurements were taken at specific intervals (0, 1, 7, and 14 days) to assess PS, PDI, and ZP. According to the results (Table 6), the developed NLCs maintained good colloidal stability with no significant changes observed in size, PDI, and ZP.

In vitro Antibacterial Studies

This research pioneers the discovery of the potent antibacterial efficacy of MON against the resistant anaerobic gram-positive *C. acnes* bacteria, paving the way for new frontiers in combating infectious skin conditions. The agar dilution method was utilized to discover the ground-breaking effects of MON and MON-NLC formulation against gram-positive bacterial strains, namely *C. acnes, S. aureus*, and *S. epidermidis*. The study's minimum inhibitory concentration (MIC) results are tabulated in Table 7, and the QC range for the reference antimicrobial agent is outlined in Table 8. The MIC_{50} of MON, MON-NLC, and MON-NLC gel was 1, 2, and 0.5 µg/mL, respectively, against the 30 human isolates of *C. acnes* bacterial strains (Table 9), whereas an MIC_{50} of 4 µg/mL was found against the gram-positive *S. aureus*, and *S. epidermidis* bacterial strains which coincide with the results of previous studies[16,17] (Table 10). These findings unveil a promising effect of MON and its formulations combating acne pathogens. A low MIC range was obtained for MON-NLC gel as compared to MON and MON-NLC (Table 9), which demonstrates an improved efficacy of the gel formulation against the resistant *C. acnes* pathogen, which could be attributed to the inclusion of hydroxyethyl cellulose (HEC) polymer. While HEC, approved as an excipient by the US Food and Drug Administration, is a biocompatible, non-ionic, and non-toxic polymer[104] used as a gelling agent, thickener, and stabilizer in formulations,[105,106] studies have suggested that cellulose polymers do not possess antibacterial properties.[107,108] The antibacterial effect is primarily produced by the antimicrobial agents loaded in the cellulose-based formulations.[107] Previously conducted research,[109–112] however, has shown that cellulose-based hydrogels, when paired with antibacterial agents, can augment their

Table 6 Optimized MON-Loaded NLC Stability Study

Time (Days)	Size (nm)	PDI	ZP (mV)
0	96.65 ± 0.94	0.129 ± 0.01	−36.50 ± 0.30
1	99.19 ± 0.13	0.12 ± 0.00	−33.67 ± 0.25
7	95.23 ± 0.27	0.19 ± 0.01	−36.93 ± 0.91
14	99.37 ± 0.62	0.11 ± 0.02	−35.60 ± 1.51

Table 7 Minimum Inhibitory Concentration (MIC) of MON, MON-NLC, and MON-NLC Gel Formulation Against 30 human Isolates of *C. acnes* Strains

Strain	MALDI IDs	MON (µg/mL)	MON-NLC (µg/mL)	MON-NLC gel (µg/mL)
00–1	*C. acnes*	1	2	0.5
00–2	*C. acnes*	1	1	0.25
00–3	*C. acnes*	1	1	0.25
00–4	*C. acnes*	4	4	1
00–5	*C. acnes*	0.5	1	0.5
00–6	*C. acnes*	0.5	1	0.5
00–7	*C. acnes*	2	2	1
00–8	*C. acnes*	0.125	0.25	0.125
00–9	*C. acnes*	0.5	1	0.25
0–10	*C. acnes*	2	2	0.5
0–11	*C. acnes*	0.5	1	0.25
0–12	*C. acnes*	24	2	1
0–13	*C. acnes*	0.5	1	0.25
0–14	*C. acnes*	1	2	0.5
0–15	*C. acnes*	1	2	1
0–16	*C. acnes*	2	2	1
0–18	*C. acnes*	2	2	1
0–19	*C. acnes*	0.125	0.5	0.125
0–20	*C. acnes*	0.125	0.5	0.125
0–21	*C. acnes*	2	2	1
0–22	*C. acnes*	2	2	1
0–23	*C. acnes*	1	0.5	0.25
0–24	*C. acnes*	2	2	1
0–25	*C. acnes*	2	2	1
0–26	*C. acnes*	1	2	1
0–27	*C. acnes*	1	2	1
0–28	*C. acnes*	1	1	0.5
0–29	*C. acnes*	2	2	1
0–30	*C. acnes*	1	1	1
0–31	*C. acnes*	1	2	1

antibacterial effectiveness. This enhancement is achieved through the polymer's natural water-absorbing capabilities, which facilitate the creation of a dense network. Consequently, this promotes better integration of the antibiotic and its slow release, thereby prolonging the duration of the antibacterial effect of the formulation.[110,113]

Table 8 QC Range and MIC of Clindamycin (Control Antimicrobial) Against *B. fragilis* ATCC 25285

QC strain	Range (µg/mL)	MIC (µg/mL)
B. fragilis ATCC 25285	0.5–2	0.5

Table 9 MIC50, MIC90, and MIC Range of MON, MON-NLC, and MON-NLC Gel Formulation Against 31 Isolates of *C. acnes* Strains

C. acnes	MON (µg/mL)	MON-NLC (µg/mL)	MON-NLC gel (µg/mL)
MIC_{50}	1	2	0.5
MIC_{90}	2	2	1
MIC Range	0.125–4	0.25–4	0.125–1

Table 10 MIC of MON, MON-NLC, and MON-NLC Gel Formulation Against *S. Aureus*, and *S. Epidermidis* Strains

Species	MON (µg/mL)	MON-NLC (µg/mL)	MON-NLC gel (µg/mL)
S. aureus ATCC 29213	4	4	4
S. epidermidis ATCC 14990	4	4	4

The novel antimicrobial efficacy of MON against gram-positive bacterial pathogens is attributed to its interference with transmembrane cation flux and dependent intracellular processes, specifically altering the balance of sodium-potassium ions, thereby shifting the intracellular pH and leading to cellular death.[114–118]

Cell Cytotoxicity Assay (MTT Assay)

To evaluate the safety of the newly developed topical MON-loaded NLC formulation, a cytotoxicity assessment was conducted using the HaCaT cell line, which has previously been utilized in research to evaluate the compatibility of topical formulations.[119–121] The MTT assay was employed in this investigation to examine the cytotoxic effects of various concentrations of MON and the MON-loaded NLC formulation on HaCaT cells (Figure 10). The results revealed a downward trend in the percentage of cell viability with increasing concentrations of MON ranging from 0.5 to 8 µg mL^{-1}. As per the International ISO 10993–5 standard for in vitro cytotoxicity assessment of biomaterials,[122] a cell viability threshold of >70% is indicative of non-cytotoxicity, which was observed for the MON-NLC formulation at 8 µg/mL, with cell viability exceeding 70%, thereby indicating substantially reduced cytotoxicity compared to MON alone. The MTT findings indicate the promise of developing the MON-loaded formulation as a safe topical therapy for treating acne at concentrations effective against acne bacteria.

Ex vivo Drug Permeation and Deposition Evaluation of MON-NLC-Gel

The ex vivo permeation and deposition assay aimed to investigate how effectively MON penetrates various skin layers using full-thickness pig skin as a model. The amount of MON deposition under infinite-dose conditions was examined from three formulations: MON-NLC, MON-NLC gel, and MON in water across the epidermis, dermis, and the receiver chamber of the Franz diffusion cell after 24 h application (Figure 11).

A significant finding was that the MON-loaded NLC gel left much less MON on the skin surface (59.50 ± 505.81 ng/cm²) as extracted from the skin wash compared to the MON-loaded NLC (14313.11 ± 118.88 ng/cm²), with a highly significant p-value of <0.0001. However, the gel formulation excelled at penetrating the epidermal layers (epidermis and stratum corneum), depositing almost twice as much MON (8180.73 ± 482.37 ng/cm²) compared to MON-NLC (4219.86 ± 388.32 ng/cm²), a statistically significant difference ($p < 0.0001$).

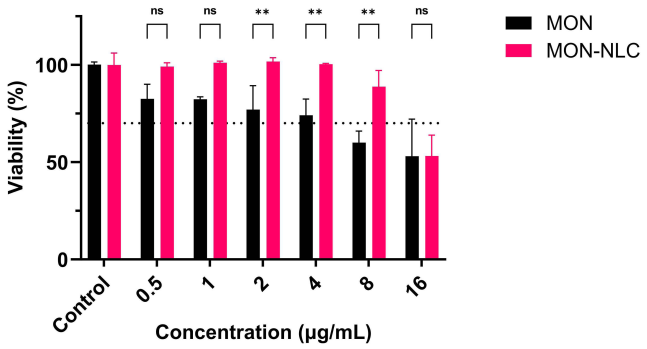

Figure 10 In vitro cellular toxicity analysis of MON and MON-NLC formulation on HaCaT cell lines using MTT assay. The dashed line indicates the industry standard cut-off for clinically safe skin cell viability against biomaterials (above 70%). Results are presented as mean ± SD from triplicate measurements. p-values were obtained via two-way analysis of variance (2way-ANOVA). ns $p > 0.05$, * $p \leq 0.05$, ** $p \leq 0.005$, and *** $p \leq 0.0008$ compared to the untreated group (control 1).

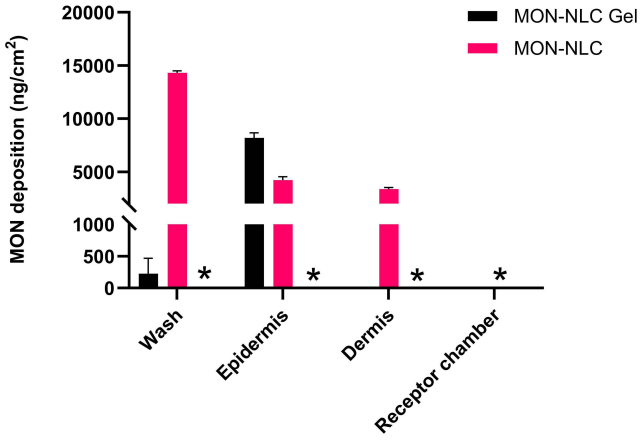

Figure 11 Ex vivo MON skin deposition and permeation using MON-NLC and MON-NLC gel on full-thickness porcine ear skin. An asterisk (*) denotes that MON was not detected in the water solution in any skin layer, MON-NLC and MON-NLC gel in the dermis, and receptor chamber. The results are presented as the mean ± SD (n = 3), with significant differences indicated by the p-value.

Even more intriguingly, the gel formulation successfully targeted the epidermis without reaching the dermis, while MON-NLC deposited a significant amount (3376.41 ± 25.47 ng/cm²) in the dermis. This selective deposition is crucial for acne treatment since pathological acne lesions primarily manifest in the epidermal hair follicular site that extends into the dermis of the skin.[123,124] Additionally, it also avoids unnecessary drug penetration into deeper skin layers and absorption into the systemic circulation, which could cause side effects.[125] In contrast, MON in water did not penetrate any skin layers due to its poor solubility and large particle size, showing no permeation across the skin barrier. This underscores the importance of using lipophilic carriers to enhance MON delivery to the intended site.

The study's most remarkable finding was the gel formulation's ability to deposit MON specifically in the epidermal layer, the target acne site,[87] without permeating the dermis or the receiver chamber. This effectiveness can be attributed to the HEC polymer, which increases retention time on the skin[126] and enhances MON's affinity for the surrounding skin environment. Additionally, the nanoparticle size is crucial in controlling the intensity of deposition and permeation, as reported previously.[127] Keeping MON localized in the epidermal layer maximizes its therapeutic effect while preventing potential side effects from deeper penetration. To confirm this, MON was quantified from the receiver chamber of the Franz cell after 24 hours of application, and no MON was detected with either the gel formulation or MON-NLC. This selective targeting highlights the gel formulation's potential for more effective and safer acne treatment.

This study utilized infinite-dose conditions, incorporating MON amounts in the formulations that exceeded the MIC values determined earlier in section 4.4, to evaluate potential side effects when administered in larger quantities. The results demonstrated that, despite the high MON concentration in the NLC formulations, no MON permeated into the deeper skin

https://doi.org/10.2147/IJN.S497108

layers from NLC formulations, as shown in Figure 11. Additionally, its safety for topical application is also demonstrated by the cell viability results, indicating that the NLC formulation was superior and safer than MON alone at such high concentrations. Further pre-clinical and clinical studies are needed to establish MON's clinical safety profile and avoid any adverse effects.

Conclusion

In this study, the antibacterial efficacy of MON was discovered against human isolates of *C. acnes*. To achieve this effect, topical delivery of MON to the target epithelial site was determined. This was achieved by formulating and characterizing MON-NLC using the CCD approach. The effect of the concentration of BM and surfactant, along with the sonication time, was evaluated on the PS, PDI, and ZP of the MON-loaded NLCs. The optimized MON-NLCs possessing PS below 100 nm and desirable PDI and ZP were transformed into a topical gel formulation that effectively delivered MON to the epithelial site compared to MON-NLCs alone, which permeated to the dermis layer and MON alone, which remained on the skin at the site of application and did not permeate to any skin layer. The results of this research, therefore, demonstrate MON's ability to be translated into a potential acne treatment and the ability of MON-NLCs to effectively achieve safe, targeted delivery of MON to hair follicular sites of infection.

Disclosure

Dr Stephen Page reports non-financial support from Luoda Pharma, during the conduct of the study; personal fees from Luoda Pharma, outside the submitted work; in addition, Dr Stephen Page has a patent AU2014214547 Methods of treating topical microbial infections issued to None. The author(s) report no conflicts of interest in this work.

References

1. Tang KWK, Millar BC, Moore JE. Antimicrobial resistance (AMR). *Br J Biomed Sci*. 2023;80:11387. doi:10.3389/bjbs.2023.11387
2. World Health Organization. Antimicrobial resistance. Available from: https://www.who.int/news-room/fact-sheets/detail/antimicrobial-resistance. Accessed February 11, 2025.
3. Dessinioti C, Katsambas A. Focus: antimicrobial resistance: antibiotics and antimicrobial resistance in acne: epidemiological trends and clinical practice considerations. *Yale J Biol Med*. 2022;95(4):429. doi:10.1016/j.jaad.2021.11.066
4. Martens E, Demain AL. The antibiotic resistance crisis, with a focus on the United States. *J Antibiot Res*. 2017;70(5):520–526. doi:10.1038/ja.2017.30
5. Goossens H, Ferech M, Vander Stichele R, Elseviers M. Outpatient antibiotic use in Europe and association with resistance: a cross-national database study. *Lancet*. 2005;365(9459):579–587. doi:10.1016/S0140-6736(05)17907-0
6. Goossens H. Antibiotic consumption and link to resistance. *Clin Microbiol Infect*. 2009;15:12–15. doi:10.1111/j.1469-0691.2009.02725.x
7. Coates P, Vyakrnam S, Eady E, Jones C, Cove J, Cunliffe W. Prevalence of antibiotic-resistant propionibacteria on the skin of acne patients: 10-year surveillance data and snapshot distribution study. *Br J Dermatol*. 2002;146(5):840–848. doi:10.1046/j.1365-2133.2002.04690.x
8. Dessinioti C, Katsambas A. Propionibacterium acnes and antimicrobial resistance in acne. *Clin Dermatol*. 2017;35(2):163–167. doi:10.1016/j.clindermatol.2016.10.008
9. Zouboulis C, Eady A, Philpott M, et al. What is the pathogenesis of acne? *Exp Dermatol*. 2005;14(2):143. doi:10.1111/j.0906-6705.2005.0285a.x
10. Haney ME, Hoehn MM. Monensin, a new biologically active compound. I. Discovery and isolation. *Antimicrob Agents Chemother*. 1967;7:349–352. doi:10.1128/AAC.7.3.349
11. Rajendran V, Ilamathi HS, Dutt S, Lakshminarayana T, Ghosh PC. Chemotherapeutic potential of monensin as an anti-microbial agent. *Curr Top Med Chem*. 2018;18(22):1976–1986. doi:10.2174/1568026619666181129141151
12. Pressman B. Ionophorous antibiotics as models for biological transport. *Fed Proc*. 1968;27:1283–1288.
13. Nachliel E, Finkelstein Y, Gutman M. The mechanism of monensin-mediated cation exchange based on real time measurements. *Biochim Biophys Acta Biomembr*. 1996;1285(2):131–145. doi:10.1016/S0005-2736(96)00149-6
14. Ben-Tal N, Sitkoff D, Bransburg-Zabary S, Nachliel E, Gutman M. Theoretical calculations of the permeability of monensin–cation complexes in model bio-membranes. *Biochim Biophys Acta Biomembr*. 2000;1466(1–2):221–233. doi:10.1016/S0005-2736(00)00156-5
15. Beckett S, Lean I, Dyson R, Tranter W, Wade L. Effects of monensin on the reproduction, health, and milk production of dairy cows. *Journal of Dairy Science*. 1998;81(6):1563–1573. doi:10.3168/jds.S0022-0302(98)75722-4
16. Stefańska J, Stępień K, Huczyński A, Tyski S. Activity of natural polyether ionophores: monensin and salinomycin against clinical Staphylococcus epidermidis strains. *Pol J Microbiol*. 2015;64(3):273–278. doi:10.5604/01.3001.0009.2122
17. Chan WY, Hickey EE, Khazandi M, Page SW, Trott DJ, Hill PB. In vitro antimicrobial activity of narasin and monensin in combination with adjuvants against pathogens associated with canine otitis externa. *Vet Dermatol*. 2020;31(2):138–e26. doi:10.1111/vde.12803
18. Lousada M, Lachnit T, Edelkamp J, et al. Exploring the human hair follicle microbiome. *Br J Dermatol*. 2021;184(5):802–815. doi:10.1111/bjd.19461
19. Makhmalzade BS, Chavoshy F. Polymeric micelles as cutaneous drug delivery system in normal skin and dermatological disorders. *J Adv Pharmaceut Technol Res*. 2018;9(1):2–8. doi:10.4103/japtr.JAPTR_314_17
20. Kim S, Day CM, Song Y, Holmes A, Garg S. Innovative topical patches for non-melanoma skin cancer: current challenges and key formulation considerations. *Pharmaceutics*. 2023;15(11):2577. doi:10.3390/pharmaceutics15112577

21. Prausnitz MR, Elias PM, Franz TJ, et al. Skin barrier and transdermal drug delivery. *Dermatology*. 2012;3:2065–2073.
22. Henri J, Burel C, Sanders P, Laurentie M. Bioavailability, distribution and depletion of monensin in chickens. *J Vet Pharmacol Ther*. 2009;32 (5):451–456. doi:10.1111/j.1365-2885.2009.01063.x
23. Patzelt A, Richter H, Knorr F, et al. Selective follicular targeting by modification of the particle sizes. *J Control Release*. 2011;150(1):45–48. doi:10.1016/j.jconrel.2010.11.015
24. Lauterbach A, Müller-Goymann CC. Comparison of rheological properties, follicular penetration, drug release, and permeation behavior of a novel topical drug delivery system and a conventional cream. *Eur J Pharm Biopharm*. 2014;88(3):614–624. doi:10.1016/j.ejpb.2014.10.001
25. Lademann J, Richter H, Meinke MC, et al. Drug delivery with topically applied nanoparticles: science fiction or reality. *Skin Pharmacol Physiol*. 2013;26(4–6):227–233. doi:10.1159/000351940
26. Ahmad Nasrollahi S, Koohestani F, Naeimifar A, Samadi A, Vatanara A, Firooz A. Preparation and evaluation of Adapalene nanostructured lipid carriers for targeted drug delivery in acne. *Dermatologic Therapy*. 2021;34(2):e14777. doi:10.1111/dth.14777
27. Jain A, Garg NK, Jain A, et al. A synergistic approach of Adapalene-loaded nanostructured lipid carriers, and vitamin C co-administration for treating acne. *Drug Dev Ind Pharm* 2016;42(6):897–905. doi:10.3109/03639045.2015.1104343
28. Kumari S, Pandita D, Poonia N, Lather V. Nanostructured lipid carriers for topical delivery of an anti-acne drug: characterization and ex vivo evaluation. *Pharm Nanotechnol*. 2015;3(2):122–133. doi:10.2174/2211738503021511161247 57
29. Chutoprapat R, Witarat J, Jongpanyangarm P, Thluai LMS, Khankaew P, Chan LW. Development of solid lipid microparticles (SLMs) containing asiatic acid for topical treatment of acne: characterization, stability, in vitro and in vivo anti-acne assessment. *Int J Pharm*. 2024;654:123980. doi:10.1016/j.ijpharm.2024.123980
30. Jain AK, Jain A, Garg NK, et al. Adapalene loaded solid lipid nanoparticles gel: an effective approach for acne treatment. *Colloids Surf B*. 2014;121:222–229. doi:10.1016/j.colsurfb.2014.05.041
31. Pawar R, Dawre S. Solid lipid nanoparticles dispersed topical hydrogel for Co-delivery of Adapalene and minocycline for acne treatment. *J Drug Deliv Sci Technol*. 2023;80:104149. doi:10.1016/j.jddst.2023.104149
32. Pokharkar VB, Mendiratta C, Kyadarkunte AY, Bhosale SH, Barhate GA. Skin delivery aspects of benzoyl peroxide-loaded solid lipid nanoparticles for acne treatment. *Ther Deliv*. 2014;5(6):635–652. doi:10.4155/tde.14.31
33. Vijayan V, Aafreen S, Sakthivel S, Reddy KR. Formulation and characterization of solid lipid nanoparticles loaded Neem oil for topical treatment of acne. *J Acute Dis*. 2013;2(4):282–286. doi:10.1016/S2221-6189(13)60144-4
34. Asyhari HF, Cabral KB, Wikantyasning ER. Optimization of Soursop (Annona muricata L.) leaf extract in nanoemulgel and antiacnes activity test against Propionibacterium acnes, Staphylococcus aureus, Staphylococcus epidermidis Bacteria. *Pharmacon*. 2023;20(2):216–225. doi:10.23917/pharmacon.v20i2.23308
35. Eid AM, Naseef H, Jaradat N, Ghanim L, Moqadeh R, Yaseen M. Antibacterial and anti-acne activity of benzoyl peroxide nanoparticles incorporated in lemongrass oil nanoemulgel. *Gels*. 2023;9(3):186. doi:10.3390/gels9030186
36. Infante VHP, Darvin ME, Maia Campos PM. Characterization and efficacy of essential oil-based cosmetic formulations for acne-prone skin. *Cosmetics*. 2023;10(6):158. doi:10.3390/cosmetics10060158
37. Samanci B, Yener FG, Değim İT. Nanoemulsions a new topical drug delivery system for the treatment of acne. *J Res Pharm*. 2023;27(1).
38. Tanessa M, Ginting CN, Chiuman L, Hutagalung MHP. Evaluation of the anti-acne effectiveness of Andaliman (Zanthoxylum acanthopodium DC) nanoemulgel in Propionibacterium acnes-induced male Wistar rats. *Jurnal Teknologi Laboratorium*. 2024;13(2):126–134. doi:10.29238/ teknolabjournal.v13i2.501
39. Arooj A, Rehman AU, Iqbal M, Naz I, Alhodaib A, Ahmed N. Development of Adapalene loaded liposome based gel for acne. *Gels*. 2023;9 (2):135. doi:10.3390/gels9020135
40. Wadaskar P, Nirale K, Rajgure M. Liposomes containing azithromycin and green tea as an anti-acne treatment: formulation and Characterization. 2023.
41. Rao MR, Deshpande S, Deshpande P. Dapsone-loaded mixed micellar gel for treatment of acne vulgaris. *AAPS Pharm Sci Tech*. 2023;24 (5):109. doi:10.1208/s12249-023-02564-1
42. Abid F, Savaliya B, Parikh A, et al. Nanotechnology and narasin: a powerful combination against acne. *Nanoscale*. 2023;15(33):13728–13739. doi:10.1039/D3NR01789C
43. Dawre S. Development and characterization of adapalene loaded microemulsion-based hydrogel for acne treatment: adapalene microemulsion. *Int J Drug Deliv Controlled Release*. 2023;2(1):38–44. doi:10.55124/jdcr.v2i1.233
44. Salem AE, Mohamed EA, Zohdy M, Elsaed WM, Abdelghani GM, Saleh NM. New insights from the integration of dapsone, flutamide, tea tree oil, and rose oil as a topical combined microemulsion for the management of Acne Vulgaris: design, development, and in vitro/in vivo characterization. *J Drug Deliv Sci Technol*. 2024;101:106276. doi:10.1016/j.jddst.2024.106276
45. Çağlar EŞ, Reis R, Karadağ AE, et al. Preparation, characterization, and in vitro evaluation of microemulsion based cream formulations for the topical treatment of acne vulgaris. *J Surfactants Deterg*. 2024.
46. Badawi NM, Yehia RM, Lamie C, Abdelrahman KA, Attia DA, Helal DA. Tackling acne vulgaris by fabrication of tazarotene-loaded essential oil-based microemulsion: in vitro and in vivo evaluation. *Int J Pharm X*. 2023;5:100185. doi:10.1016/j.ijpx.2023.100185
47. Shamma RN, Aburahma MH. Follicular delivery of spironolactone via nanostructured lipid carriers for management of alopecia. *Int j Nanomed*. 2014;5449–5460. doi:10.2147/IJN.S73010
48. Pereira MN, Tolentino S, Pires FQ, et al. Nanostructured lipid carriers for hair follicle-targeted delivery of clindamycin and rifampicin to hidradenitis suppurativa treatment. *Colloids Surf B*. 2021;197:111448. doi:10.1016/j.colsurfb.2020.111448
49. Malik DS, Kaur G. Exploring therapeutic potential of azelaic acid loaded NLCs for the treatment of acne vulgaris. *J Drug Deliv Sci Technol*. 2020;55:101418. doi:10.1016/j.jddst.2019.101418
50. Lin Y-K, Al-Suwayeh SA, Leu Y-L, Shen F-M, Fang J-Y. Squalene-containing nanostructured lipid carriers promote percutaneous absorption and hair follicle targeting of diphencyprone for treating alopecia areata. *Pharm Res*. 2013;30:435–446. doi:10.1007/s11095-012-0888-0
51. Aljuffali IA, Sung CT, Shen F-M, Huang C-T, Fang J-Y. Squarticles as a lipid nanocarrier for delivering diphencyprone and minoxidil to hair follicles and human dermal papilla cells. *AAPS J*. 2014;16:140–150. doi:10.1208/s12248-013-9550-y
52. Iqbal MA, Md S, Sahni JK, Baboota S, Dang S, Ali J. Nanostructured lipid carriers system: recent advances in drug delivery. *J Drug Targeting*. 2012;20(10):813–830. doi:10.3109/1061186X.2012.716845

53. Kim S, Abdella S, Abid F, et al. Development and optimization of imiquimod-loaded nanostructured lipid carriers using a hybrid design of experiments approach. *Int j Nanomed*. 2023;18:1007–1029. doi:10.2147/IJN.S400610
54. Gratieri T, Krawczyk-Santos AP, da Rocha PB, Gelfuso GM, Marreto RN, Taveira SF. SLN-and NLC-encapsulating antifungal agents: skin drug delivery and their unexplored potential for treating onychomycosis. *Curr Pharm Des*. 2017;23(43):6684–6695. doi:10.2174/1381612823666171115112745
55. Santos G, Angelo T, Andrade L, et al. The role of formulation and follicular pathway in voriconazole cutaneous delivery from liposomes and nanostructured lipid carriers. *Colloids Surf B*. 2018;170:341–346. doi:10.1016/j.colsurfb.2018.06.037
56. Czajkowska-Kośnik A, Szekalska M, Winnicka K. Nanostructured lipid carriers: a potential use for skin drug delivery systems. *Pharmacol Rep*. 2019;71(1):156–166. doi:10.1016/j.pharep.2018.10.008
57. Pires FQ, da Silva JKR, Sa-Barreto LL, Gratieri T, Gelfuso GM, Cunha-Filho M. Lipid nanoparticles as carriers of cyclodextrin inclusion complexes: a promising approach for cutaneous delivery of a volatile essential oil. *Colloids Surf B*. 2019;182:110382. doi:10.1016/j.colsurfb.2019.110382
58. Garcês A, Amaral M, Lobo JS, Silva AC. Formulations based on solid lipid nanoparticles (SLN) and nanostructured lipid carriers (NLC) for cutaneous use: a review. *Eur J Pharm Sci*. 2018;112:159–167. doi:10.1016/j.ejps.2017.11.023
59. Silva LAD, Andrade LM, de Sá FAP, et al. Clobetasol-loaded nanostructured lipid carriers for epidermal targeting. *J Pharm Pharmacol*. 2016;68(6):742–750. doi:10.1111/jphp.12543
60. Beloqui A, Solinís MÁ, Rodríguez-Gascón A, Almeida AJ, Préat V. Nanostructured lipid carriers: promising drug delivery systems for future clinics. *Nanomedicine*. 2016;12(1):143–161. doi:10.1016/j.nano.2015.09.004
61. Yousef S, Mohammed Y, Namjoshi S, Grice J, Sakran W, Roberts M. Mechanistic evaluation of hydration effects on the human epidermal permeation of salicylate esters. *AAPS J*. 2017;19:180–190. doi:10.1208/s12248-016-9984-0
62. Shah M, Agrawal Y. High throughput screening: an in silico solubility parameter approach for lipids and solvents in SLN preparations. *Pharm Dev Technol*. 2013;18(3):582–590. doi:10.3109/10837450.2011.635150
63. Makoni PA, Ranchhod J, WaKasongo K, Khamanga SM, Walker RB. The use of quantitative analysis and Hansen solubility parameter predictions for the selection of excipients for lipid nanocarriers to be loaded with water soluble and insoluble compounds. *Saudi Pharm J*. 2020;28(3):308–315. doi:10.1016/j.jsps.2020.01.010
64. Iqubal MK, Iqubal A, Imtiyaz K, et al. Combinatorial lipid-nanosystem for dermal delivery of 5-fluorouracil and resveratrol against skin cancer: delineation of improved dermatokinetics and epidermal drug deposition enhancement analysis. *Eur J Pharm Biopharm*. 2021;163:223–239. doi:10.1016/j.ejpb.2021.04.007
65. Rathod VR, Shah DA, Dave RH. Systematic implementation of quality-by-design (QbD) to develop NSAID-loaded nanostructured lipid carriers for ocular application: preformulation screening studies and statistical hybrid-design for optimization of variables. *Drug Dev Ind Pharm*. 2020;46(3):443–455. doi:10.1080/03639045.2020.1724135
66. Al-Mayahy MH, Sabri AH, Rutland CS, et al. Insight into imiquimod skin permeation and increased delivery using microneedle pre-treatment. *Eur J Pharm Biopharm*. 2019;139:33–43. doi:10.1016/j.ejpb.2019.02.006
67. Sivadasan D, Sultan MH, Madkhali OA, Alsabei SH, Alessa AA. Stealth liposomes (PEGylated) containing an anticancer drug camptothecin: in vitro characterization and in vivo pharmacokinetic and tissue distribution study. *Molecules*. 2022;27(3):1086. doi:10.3390/molecules27031086
68. CLSI. Methods for Antimicrobial Susceptibility Testing of Anaerobic Bacteria, 9th Edition. CLSI document M11Ed 9E2018.
69. Kaithwas V, Dora CP, Kushwah V, Jain S. Nanostructured lipid carriers of olmesartan medoxomil with enhanced oral bioavailability. *Colloids Surf B*. 2017;154:10–20. doi:10.1016/j.colsurfb.2017.03.006
70. Mukherjee S, Ray S, Thakur R. Solid lipid nanoparticles: a modern formulation approach in drug delivery system. *Indian J Pharm Sci*. 2009;71(4):349. doi:10.4103/0250-474X.57282
71. Moghddam SMM, Ahad A, Aqil M, Imam SS, Sultana Y. Optimization of nanostructured lipid carriers for topical delivery of nimesulide using Box–Behnken design approach. *Artif Cells Nanomed Biotechnol*. 2017;45(3):617–624. doi:10.3109/21691401.2016.1167699
72. Ghate VM, Lewis SA, Prabhu P, Dubey A, Patel N. Nanostructured lipid carriers for the topical delivery of tretinoin. *Eur J Pharm Biopharm*. 2016;108:253–261. doi:10.1016/j.ejpb.2016.07.026
73. Noor NM, Umar S, Abdul-Aziz A, Sheikh K, Somavarapu S. Engineered Dutasteride-Lipid Based Nanoparticle (DST-LNP) system using oleic and stearic acid for topical delivery. *Bioengineering*. 2022;9(1):11. doi:10.3390/bioengineering9010011
74. Patel D, Dasgupta S, Dey S, Roja Ramani Y, Ray S, Mazumder B. Nanostructured lipid carriers (NLC)-based gel for the topical delivery of aceclofenac: preparation, characterization, and in vivo evaluation. *Sci Pharm*. 2012;80(3):749–764. doi:10.3797/scipharm.1202-12
75. Sachan AK, Gupta A, Arora M. Formulation & characterization of nanostructured lipid carrier (NLC) based gel for topical delivery of etoricoxib. *J Drug Delivery Ther*. 2016;6(2):4–13. doi:10.22270/jddt.v6i2.1222
76. Almeida EDP, Dipieri LV, Rossetti FC, et al. Skin permeation, biocompatibility and antitumor effect of chloroaluminum phthalocyanine associated to oleic acid in lipid nanoparticles. *Photodiagn Photodyn Ther*. 2018;24:262–273. doi:10.1016/j.pdpdt.2018.10.002
77. Kelidari H, Saeedi M, Akbari J, et al. Formulation optimization and in vitro skin penetration of spironolactone loaded solid lipid nanoparticles. *Colloids Surf B*. 2015;128:473–479. doi:10.1016/j.colsurfb.2015.02.046
78. Mehnert W, Mäder K. Solid lipid nanoparticles: production, characterization and applications. *Adv Drug Delivery Rev*. 2012;64:83–101. doi:10.1016/j.addr.2012.09.021
79. Severino P, Pinho SC, Souto EB, Santana MH. Polymorphism, crystallinity and hydrophilic–lipophilic balance of stearic acid and stearic acid–capric/caprylic triglyceride matrices for production of stable nanoparticles. *Colloids Surf B*. 2011;86(1):125–130. doi:10.1016/j.colsurfb.2011.03.029
80. Ciftci ON, Temelli F. Melting point depression of solid lipids in pressurized carbon dioxide. *J Supercrit Fluids*. 2014;92:208–214. doi:10.1016/j.supflu.2014.05.009
81. Fidorra M, Heimburg T, Seeger H. Melting of individual lipid components in binary lipid mixtures studied by FTIR spectroscopy, DSC and Monte Carlo simulations. *Biochim Biophys Acta Biomembr*. 2009;1788(3):600–607. doi:10.1016/j.bbamem.2008.12.003
82. Guo Z, Jia X, Miao S, Chen B, Lu X, Zheng B. Structural and thermal properties of amylose–fatty acid complexes prepared via high hydrostatic pressure. *Food Chem*. 2018;264:172–179. doi:10.1016/j.foodchem.2018.05.032

83. Imran M, Iqubal MK, Imtiyaz K, et al. Topical nanostructured lipid carrier gel of quercetin and resveratrol: formulation, optimization, in vitro and ex vivo study for the treatment of skin cancer. *Int J Pharm*. 2020;587:119705. doi:10.1016/j.ijpharm.2020.119705
84. Mahant S, Rao R, Souto EB, Nanda S. Analytical tools and evaluation strategies for nanostructured lipid carrier-based topical delivery systems. *Expert Opin Drug Deliv*. 2020;17(7):963–992. doi:10.1080/17425247.2020.1772750
85. Shah B, Khunt D, Bhatt H, Misra M, Padh H. Application of quality by design approach for intranasal delivery of rivastigmine loaded solid lipid nanoparticles: effect on formulation and characterization parameters. *Eur J Pharm Sci*. 2015;78:54–66. doi:10.1016/j.ejps.2015.07.002
86. Souto E, Wissing S, Barbosa C, Müller R. Development of a controlled release formulation based on SLN and NLC for topical clotrimazole delivery. *Int J Pharm*. 2004;278(1):71–77. doi:10.1016/j.ijpharm.2004.02.032
87. Lademann J, Knorr F, Richter H, et al. Hair follicles as a target structure for nanoparticles. *J Innov Opt Health Sci*. 2015;8(04):1530004. doi:10.1142/S1793545815300049
88. Lademann J, Richter H, Schanzer S, et al. Penetration and storage of particles in human skin: perspectives and safety aspects. *Eur J Pharm Biopharm*. 2011;77(3):465–468. doi:10.1016/j.ejpb.2010.10.015
89. Patzelt A, Lademann J. Drug delivery to hair follicles. *Expert Opin Drug Deliv*. 2013;10(6):787–797.
90. Su R, Fan W, Yu Q, et al. Size-dependent penetration of nanoemulsions into epidermis and hair follicles: implications for transdermal delivery and immunization. *Oncotarget*. 2017;8(24):38214. doi:10.18632/oncotarget.17130
91. Jain K, Sood S, Gowthamarajan K. Optimization of artemether-loaded NLC for intranasal delivery using central composite design. *Drug Delivery*. 2015;22(7):940–954. doi:10.3109/10717544.2014.885999
92. Wu K-W, Sweeney C, Dudhipala N, et al. Primaquine loaded solid lipid nanoparticles (SLN), nanostructured lipid carriers (NLC), and nanoemulsion (NE): effect of lipid matrix and surfactant on drug entrapment, in vitro release, and ex vivo hemolysis. *AAPS Pharm Sci Tech*. 2021;22:1–12. doi:10.1208/s12249-021-02108-5
93. McClements DJ. Crystals and crystallization in oil-in-water emulsions: implications for emulsion-based delivery systems. *Adv Colloid Interface Sci*. 2012;174:1–30. doi:10.1016/j.cis.2012.03.002
94. Taha E, Nour SA, Mamdouh W, et al. Cod liver oil nano-structured lipid carriers (Cod-NLCs) as a promising platform for nose to brain delivery: preparation, in vitro optimization, ex vivo cytotoxicity & in vivo biodistribution utilizing radioiodinated zopiclone. *Int J Pharm X*. 2023;5:100160. doi:10.1016/j.ijpx.2023.100160
95. Yang Z, He Q, Ismail BB, Hu Y, Guo M. Ultrasonication induced nano-emulsification of thyme essential oil: optimization and antibacterial mechanism against Escherichia coli. *Food Control*. 2022;133:108609. doi:10.1016/j.foodcont.2021.108609
96. Musielak E, Feliczak-Guzik A, Nowak I. Optimization of the conditions of solid lipid nanoparticles (SLN) synthesis. *Molecules*. 2022;27(7):2202. doi:10.3390/molecules27072202
97. Doktorovova S, Souto EB. Nanostructured lipid carrier-based hydrogel formulations for drug delivery: a comprehensive review. *Expert Opin Drug Deliv*. 2009;6(2):165–176. doi:10.1517/17425240802712590
98. Remiro PDFR, e Rosa PDTV, Moraes AM. Effect of process variables on imiquimod micronization using a supercritical antisolvent (SAS) precipitation technique. *J Supercrit Fluids*. 2022;181:105500. doi:10.1016/j.supflu.2021.105500
99. Shah RM, Eldridge DS, Palombo EA, Harding IH. Stability mechanisms for microwave-produced solid lipid nanoparticles. *Colloids Surf A*. 2022;643:128774. doi:10.1016/j.colsurfa.2022.128774
100. Surolia R, Pachauri M, Ghosh P. Preparation and characterization of monensin loaded PLGA nanoparticles: in vitro anti-malarial activity against plasmodium falciparum. *J Biomed Nanotechnol*. 2012;8:172–181. doi:10.1166/jbn.2012.1366
101. Zhu J, Liu B, Li L, et al. Simple and green fabrication of super-hydrophobic surface by one-step immersion for continuous oil/water separation. *J Phys Chem A*. 2016;120:5617–5623. doi:10.1021/acs.jpca.6b06146
102. Abdella S, Kim S, Afinjuomo F, Song Y, Upton R, Garg S. Combining the potential of 3D printed buccal films and nanostructured lipid carriers for personalised cannabidiol delivery. *Drug Delivery Transl Res*. 2024;14(4):984–1004. doi:10.1007/s13346-023-01446-0
103. Lukić M, Pantelić I, Savić SD. Towards optimal ph of the skin and topical formulations: from the current state of the art to tailored products. *Cosmetics*. 2021;8(3):69. doi:10.3390/cosmetics8030069
104. Noreen A, Zia KM, Tabasum S, Aftab W, Shahid M, Zuber M. Hydroxyethylcellulose-g-poly (lactic acid) blended polyurethanes: preparation, characterization and biological studies. *Int J Biol Macromol*. 2020;151:993–1003. doi:10.1016/j.ijbiomac.2019.10.254
105. Ho HN, Le HH, Le TG, et al. Formulation and characterization of hydroxyethyl cellulose-based gel containing metronidazole-loaded solid lipid nanoparticles for buccal mucosal drug delivery. *Int J Biol Macromol*. 2022;194:1010–1018. doi:10.1016/j.ijbiomac.2021.11.161
106. El Fawal GF, Abu-Serie MM, Hassan MA, Elnouby MS. Hydroxyethyl cellulose hydrogel for wound dressing: fabrication, characterization and in vitro evaluation. *Int J Biol Macromol*. 2018;111:649–659. doi:10.1016/j.ijbiomac.2018.01.040
107. Bao Y, He J, Song K, Guo J, Zhou X, Liu S. Functionalization and antibacterial applications of cellulose-based composite hydrogels. *Polymers*. 2022;14(4):769. doi:10.3390/polym14040769
108. Alavi M. Modifications of microcrystalline cellulose (MCC), nanofibrillated cellulose (NFC), and nanocrystalline cellulose (NCC) for antimicrobial and wound healing applications. *e-Polymers*. 2019;19(1):103–119. doi:10.1515/epoly-2019-0013
109. Yadollahi M, Gholamali I, Namazi H, Aghazadeh M. Synthesis and characterization of antibacterial carboxymethyl cellulose/ZnO nanocomposite hydrogels. *Int J Biol Macromol*. 2015;74:136–141. doi:10.1016/j.ijbiomac.2014.11.032
110. Sun Y, Wang J, Li D, Cheng F. The recent progress of the cellulose-based antibacterial hydrogel. *Gels*. 2024;10(2):109. doi:10.3390/gels10020109
111. Suchomel P, Kvitek L, Panacek A, et al. Comparative study of antimicrobial activity of AgBr and Ag nanoparticles (NPs). *PLoS One*. 2015;10(3):e0119202. doi:10.1371/journal.pone.0119202
112. George D, Maheswari PU, Sheriffa Begum KMM, Arthanareeswaran G. Biomass-derived dialdehyde cellulose cross-linked chitosan-based nanocomposite hydrogel with phytosynthesized zinc oxide nanoparticles for enhanced curcumin delivery and bioactivity. *J Agric Food Chem*. 2019;67(39):10880–10890. doi:10.1021/acs.jafc.9b01933
113. Sabbagh F, Muhamad II. Acrylamide-based hydrogel drug delivery systems: release of Acyclovir from MgO nanocomposite hydrogel. *J Taiwan Inst Chem Eng*. 2017;72:182–193. doi:10.1016/j.jtice.2016.11.032
114. Russell JB, Strobel H. Effect of ionophores on ruminal fermentation. *Appl Environ Microbiol*. 1989;55(1):1–6. doi:10.1128/aem.55.1.1-6.1989
115. Pressman BC. Biological applications of ionophores. *Annu Rev Biochem*. 1976;45(1):501–530. doi:10.1146/annurev.bi.45.070176.002441

116. Kevin Ii DA, Meujo DA, Hamann MT. Polyether ionophores: broad-spectrum and promising biologically active molecules for the control of drug-resistant bacteria and parasites. *Expert Opin Drug Discov*. 2009;4(2):109–146. doi:10.1517/17460440802661443
117. Callaway T, Edrington T, Rychlik J, et al. Ionophores: their use as ruminant growth promotants and impact on food safety. *Curr Issues Intestinal Microbiol*. 2003;4(2):43–51.
118. Butaye P, Devriese LA, Haesebrouck F. Antimicrobial growth promoters used in animal feed: effects of less well known antibiotics on gram-positive bacteria. *Clin Microbiol Rev*. 2003;16(2):175–188. doi:10.1128/CMR.16.2.175-188.2003
119. Ramata-Stunda A, Boroduskis M, Vorobjeva V, Ancans J. Cell and tissue culture-based in vitro test systems for evaluation of natural skin care product ingredients. *Environ Exp Biol*. 2013;11:159–177.
120. Józsa L, Ujhelyi Z, Vasvári G, et al. Formulation of creams containing spirulina platensis powder with different nonionic surfactants for the treatment of acne vulgaris. *Molecules*. 2020;25(20):4856. doi:10.3390/molecules25204856
121. Colombo I, Sangiovanni E, Maggio R, et al. HaCaT cells as a reliable in vitro differentiation model to dissect the inflammatory/repair response of human keratinocytes. *Mediators Inflamm*. 2017;2017:1–12. doi:10.1155/2017/7435621
122. Iso I. 10993–5: 2009 Biological evaluation of medical devices—part 5: tests for in vitro cytotoxicity. *Int Organ Stand Geneva*. 2009;34.
123. Martel JL, Miao JH, Badri T. Anatomy, hair follicle. 2017.
124. Wang Z, Liu L, Xiang S, et al. Formulation and characterization of a 3D-printed cryptotanshinone-loaded niosomal hydrogel for topical therapy of acne. *AAPS Pharm Sci Tech*. 2020;21:1–13. doi:10.1208/s12249-020-01677-1
125. Souto EB, Baldim I, Oliveira WP, et al. SLN and NLC for topical, dermal, and transdermal drug delivery. *Expert Opin Drug Deliv*. 2020;17(3):357–377. doi:10.1080/17425247.2020.1727883
126. Jones DS, Woolfson AD, Brown AF. Textural, viscoelastic and mucoadhesive properties of pharmaceutical gels composed of cellulose polymers. *Int J Pharm*. 1997;151(2):223–233. doi:10.1016/S0378-5173(97)04904-1
127. Papakostas D, Rancan F, Sterry W, Blume-Peytavi U, Vogt A. Nanoparticles in dermatology. *Arch Dermatol Res*. 2011;303:533–550. doi:10.1007/s00403-011-1163-7